

# **An Effective Model of the Retinoic Acid Induced HL-60 Differentiation Program**

Ryan Tasseff, Holly A. Jensen, Johanna Congleton<sup>†</sup>, Wei Dai, Katherine Rogers, Adithya Sagar, Rodica P. Bunaciu<sup>†</sup>, Andrew Yen<sup>†</sup>, and Jeffrey D. Varner\*

Robert Frederick Smith School of Chemical and Biomolecular Engineering and <sup>†</sup>Department of Biomedical Sciences, Cornell University, Ithaca NY 14853

**Running Title:** Effective modeling of HL-60 differentiation

**To be submitted:** ?

\*Corresponding author:

Jeffrey D. Varner,

Professor, Robert Frederick Smith School of Chemical and Biomolecular Engineering,  
244 Olin Hall, Cornell University, Ithaca NY, 14853

Email: jdv27@cornell.edu

Phone: (607) 255 - 4258

Fax: (607) 255 - 9166

## **Abstract**

In this study, we present an effective model All-Trans Retinoic Acid (ATRA)-induced differentiation of HL-60 cells. The model describes a key architectural feature of ATRA-induced differentiation, positive feedback between an ATRA-inducible signalsome complex involving many proteins including Vav1, a guanine nucleotide exchange factor, and the activation of the mitogen activated protein kinase (MAPK) cascade. The model, which was developed by integrating logical rules with kinetic modeling, was significantly smaller than previous models. However, despite its simplicity, it captured key features of ATRA induced differentiation of HL-60 cells. We identified an ensemble of effective model parameters using measurements taken from ATRA-induced HL-60 cells. Using these parameters, model analysis predicted that MAPK activation was bistable as a function of ATRA exposure. Conformational experiments supported ATRA-induced bistability. These findings, combined with other literature evidence, suggest that positive feedback is central to a diversity of cell fate programs.

## **1 Introduction**

2 Understanding the architecture of differentiation programs is an important therapeutic  
3 challenge. Differentiation induction chemotherapy (DIC), using agents such as the vita-  
4 min A derivative all-trans retinoic acid (ATRA), is a promising approach for the treatment  
5 of many cancers (1–3). For example, ATRA treatment induces remission in 80–90% of  
6 promyelocytic leukemia (APL) PML-RAR $\alpha$ -positive patients (4), thereby transforming a  
7 fatal diagnosis into a manageable disease. However, remission is sometimes not durable  
8 and relapsed cases exhibit emergent ATRA resistance (5, 6). To understand the basis of  
9 this resistance, we must first understand the ATRA-induced differentiation program. To-  
10 ward this challenge, lessons learned in model systems, such as the lineage-uncommitted  
11 human myeloblastic cell line HL-60, could inform our analysis of the more complex dif-  
12 ferentiation programs occurring in patients. Patient derived HL-60 leukemia cells have  
13 been a durable experimental model since the 1970's to study differentiation (7). HL-60  
14 undergoes cell cycle arrest and either myeloid or monocytic differentiation following stim-  
15 ulation; ATRA induces G1/G0-arrest and myeloid differentiation in HL-60 cells, while 1,25-  
16 dihydroxy vitamin D3 (D3) induces arrest and monocytic differentiation. Commitment to  
17 cell cycle arrest and differentiation requires approximately 48 hr of treatment, during which  
18 HL-60 cells undergo two division cycles.

19 Sustained mitogen-activated protein kinase (MAPK) activation is a defining feature of  
20 ATRA-induced HL-60 differentiation. ATRA drives sustained MEK-dependent activation  
21 of the Raf/MEK/ERK pathway, leading to arrest and differentiation (8). MEK inhibition re-  
22 sults in the loss of ERK and Raf phosphorylation, and the failure to arrest and differentiate  
23 (9). ATRA (and its metabolites) are ligands for the hormone activated nuclear transcrip-  
24 tion factors retinoic acid receptor (RAR) and retinoid X receptor (RXR) (10). RAR/RXR  
25 activation is necessary for ATRA-induced Raf phosphorylation (9), and the formation of  
26 an ATRA-inducible signalsome complex at the membrane which drives MAPK activation

27 through a yet to be identified kinase activity. While the makeup of the signalsome com-  
28 plex is not yet known, we do know that it is composed of Src family kinases Fgr and Lyn,  
29 PI3K, c-Cbl, Slp76, and KSR, as well as IRF-1 transcription factors (11–15). Signalsome  
30 formation and activity is driven by ATRA-induced expression of CD38 and the putative  
31 heterotrimeric Gq protein-coupled receptor BLR1 (16, 17). BLR1, identified as an early  
32 ATRA (or D3)-inducible gene using differential display (18), is necessary for MAPK ac-  
33 tivation and differentiation (17), and is also involved with signalsome activity. Studies  
34 of the BLR1 promoter identified a 5' 17bp GT box approximately 1 kb upstream of the  
35 transcriptional start that conferred ATRA responsiveness (17). Members of the BLR1  
36 transcriptional activator complex, e.g. NFATc3 and CREB, are phosphorylated by ERK,  
37 JNK or p38 MAPK family members suggesting positive feedback between the signalsome  
38 and MAPK activation (19). BLR1 overexpression enhanced Raf phosphorylation and ac-  
39 celerated terminal differentiation, while Raf inhibition reduced BLR1 expression and dif-  
40 ferentiation (20). BLR1 knock-out cells failed to activate Raf or differentiate in the pres-  
41 ence of ATRA (20). Interestingly, both the knockdown or inhibition of Raf, also reduced  
42 BLR1 expression and functional differentiation (20). Thus, the expression of signalsome  
43 components e.g., BLR1 was Raf dependent, while Raf activation depended upon the sig-  
44 nalsome. A recent computational study of ATRA-induced differentiation in HL-60 cells  
45 suggested that the BLR1-MAPK positive feedback circuit was sufficient to explain ATRA-  
46 induced sustained MAPK activation, and the expression of a limited number of functional  
47 differentiation markers (21). Model analysis also suggested that Raf was the most distinct  
48 of the MAPK proteins. However, this previous study developed and analyzed a complex  
49 model, thus leaving open the critical question of what is the minimal positive feedback  
50 circuit required to drive ATRA-induced differentiation.

51 In this study, we explored this question using a minimal mathematical model of the  
52 key architectural feature of ATRA induced differentiation of HL-60 cells, namely positive

53 feedback between an ATRA-inducible signalsome complex and MAPK activation. The  
54 ATRA responsive signalsome-MAPK circuit was then used to drive a downstream gene  
55 expression program which encoded for the expression of functional differentiation mark-  
56 ers. The effective model used a novel framework which integrated logical rules with ki-  
57 netic modeling to describe gene expression and protein regulation, while largely relying  
58 upon biophysical parameters from the literature. This formulation significantly reduced  
59 the size and complexity of the model compared to the previous study of Tasseff et al.,  
60 while increasing the breadth of the biology described (21). The effective model, despite  
61 its simplicity, captured key features of ATRA induced differentiation of HL-60 cells. Model  
62 analysis predicted the bistability of MAPK activation as a function of ATRA exposure; con-  
63 formational experiments supported ATRA-induced bistability. Model simulations were also  
64 consistent with measurements of the influence of MAPK inhibitors, and the failure of BLR1  
65 knockout cells to differentiate when exposed to ATRA. Lastly, we showed by through im-  
66 munoprecipitation studies, that the guanine nucleotide exchange factor Vav1 is potentially  
67 a new ATRA-inducible member of the signalsome complex. Taken together, these findings  
68 when combined with other literature evidence, suggested that positive feedback architec-  
69 tures are central to differentiation programs generally, and necessary for ATRA-induced  
70 differentiation.

71 **Results**

72 We constructed an effective model of ATRA-induced HL-60 differentiation which described  
73 signaling and gene expression events following the addition of ATRA (Fig. 1). The model  
74 connectivity was developed from literature and the studies presented here (Table 1). We  
75 decomposed the ATRA program into three modules; a signal initiation module that sensed  
76 and transformed the ATRA signal into activated cRaf-pS621 and the ATRA-RXR/RAR  
77 (Trigger) signals (Fig. 1A); a signal integration module that controlled the expression of  
78 upstream transcription factors given cRaf-pS621 and activated Trigger signals (Fig. 1B);  
79 and a phenotype module which encoded the expression of functional differentiation mark-  
80 ers from the ATRA-inducible transcription factors (Fig. 1C). Each component of these  
81 modules was described by a mRNA and protein balance equation. Additionally, the sig-  
82 nal initiation module also described the abundance of activated species e.g., Trigger and  
83 cRaf-pS621 whose values were derived from unactivated Trigger and cRaf protein levels.  
84 Lastly, because the population of HL-60 cells was dividing (at least before ATRA-induced  
85 cell cycle arrest), we also considered a dilution term in all balance equations. The sig-  
86 nal initiation module contained nine differential equations, while the signal integration and  
87 phenotype modules were collectively encoded by 54 differential equations. Model param-  
88 eters were taken literature (Table 2), or estimated from experimental data using heuristic  
89 optimization (see materials and methods).

90 The signal initiation module recapitulated sustained signalsome and MAPK activation  
91 following exposure to  $1\mu\text{M}$  ATRA (Fig. 2A-B). An ensemble of effective model param-  
92 eters was estimated by minimizing the difference between simulations and time-series  
93 measurements of BLR1 mRNA and cRaf-pS621 following the addition of  $1\mu\text{M}$  ATRA. We  
94 focused on the S621 phosphorylation site of cRaf since enhanced phosphorylation at  
95 this site is a defining characteristic of sustained MAPK activation in HL-60. The effective  
96 model captured both ATRA-induced BLR1 expression (Fig. 2A) and sustained phospho-

97 phosphorylation of cRaf-pS621 (Fig. 2B) in a growing population of HL-60 cells. Together, the  
98 reinforcing positive feedback between the signalsome and MAPK led to sustained activation  
99 over multiple cellular generations. However, the effective model failed to capture the  
100 decline of BLR1 message after 48 hr of ATRA exposure. This suggested that we captured  
101 the logic leading to the onset of differentiation, but failed to describe program shutdown.  
102 Next, we tested the response of the signal initiation module to different ATRA dosages.

103 The signal initiation model was bistable with respect to ATRA induction (Fig. 2C-D).  
104 Phaseplane analysis predicted two stable steady-states when ATRA was present below  
105 a critical threshold, and only a single steady-state above the threshold (Fig. 2C). In the  
106 lower stable state, neither the signalsome nor cRaf-pS621 were present (thus, the differ-  
107 entiation program was deactivated). However, at the high stable state, both the signal-  
108 some and cRaf-pS621 were present, allowing for sustained activation and differentiation.  
109 Interestingly, when ATRA was above a critical threshold, only the activated state was ac-  
110 cessible (Fig. 2D). To test these findings, we first identified the ATRA threshold. We  
111 exposed HL-60 cells to different ATRA concentrations for 72 hr (Fig. 2E). Morphological  
112 changes associated with differentiation were visible for ATRA  $\geq$  0.25  $\mu$ M, suggesting the  
113 critical ATRA threshold was near this concentration. Next, we conducted ATRA washout  
114 experiments to determine if activated cells remained activated in the absence of ATRA.  
115 HL-60 cells locked into an activated state remained activated following ATRA withdraw-  
116 (Fig. 3). This sustained activation resulted from reinforcing feedback between the sig-  
117 nalsome and the MAPK pathway. Thus, following activation, if we inhibited or removed  
118 elements from the signal initiation module we expected the signalsome and MAPK signals  
119 to decay. We simulated ATRA induced activation in the presence of kinase inhibitors, and  
120 without key circuit elements. Consistent with experimental results using multiple MAPK  
121 inhibitors, ATRA activation in the presence of MAPK inhibitors lowered the steady-state  
122 value of signalsome (Fig. 3A). In the presence of BLR1, the signalsome and cRaf-pS621

signals were maintained following ATRA withdraw (Fig. 3B, gray). On the other hand, BLR1 deletion removed the ability of the circuit to maintain a sustained MAPK response following the withdraw of ATRA (Fig. 3B, blue). Lastly, washout experiments in which cells were exposed to  $1\mu\text{M}$  ATRA for 24 hr, and then transferred to fresh media without ATRA, confirmed the persistence of the self sustaining activated state for up to 144 hr (Fig. 3C). Thus, these experiments confirmed that reinforcing positive feedback likely drives the ATRA-induced differentiation program. Next, we analyzed the ATRA-induced downstream gene expression program following signalsome and cRaf activation.

The signal integration and phenotype modules described ATRA-induced gene expression in wild-type HL-60 cells (Fig. 4). The signal initiation module produced two outputs, activated Trigger and cRaf-pS621 which drove the expression of ATRA-induced transcription factors, which then in turn activated the phenotypic program. In particular, Trigger (a surrogate for the RAR $\alpha$ /RXR transcriptional complex) regulated the expression of the transcription factors CCATT/enhancer binding protein  $\alpha$  (C/EBP $\alpha$ ), PU.1, and EGR1. In turn, these transcription factors, in combination with cRaf-pS621, regulated the expression of downstream phenotypic markers such as CD38, CD11b or P47Phox. We assembled the connectivity of the signal integration and phenotypic programs driven by Trigger and cRaf-pS621 from literature (Table 1). We estimated the parameters for the signal initiation, and phenotype modules from steady-state and dynamic measurements of transcription factor and phenotypic marker expression following the addition of ATRA (22–25). However, the bulk of the model parameters were taken from directly from literature (26) and were not estimated in this study (see materials and methods). The model simulations captured the time dependent expression of CD38 and CD11b following the addition ATRA (Fig. 4A), and the steady-state for signal integration and phenotypic markers (Fig. 4B). Lastly, we used the *predicted* values of the p21 and E2F protein abundance to estimate a black-box model of ATRA-induced G0 arrest (Fig. 5). The phenotype module predicted p21

149 expression significantly increased and E2F expression decreased, in response to ATRA  
150 exposure (Fig. 5A). We then used the ratio of these values in a polynomial model to cal-  
151 culate the fraction of HL-60 cells in G0 arrest following the addition of ATRA (Fig. 5B). The  
152 third-order polynomial model captured the trend in measured G0-arrest values as a func-  
153 tion of time, and was robust to uncertainty in the measured data (Fig. 5B, gray). Taken  
154 together, the output of the signal integration and phenotypic modules was consistent with  
155 time-series and steady-state measurements, thereby validating the assumed molecular  
156 connectivity. Moreover, outputs from the phenotype module described the trend in ATRA-  
157 induced G0 cell cycle arrest. Next, we explored which nodes and interactions between  
158 nodes in the signal integration module most influenced the system response.

159 The PU.1 and AP1 proteins were important regulators of ATRA-induced signal inte-  
160 gration and phenotypic change (Fig. 6). We conducted pairwise knockout simulations of  
161 genes in the signal integration and phenotype modules to estimate which nodes controlled  
162 the processing of the Trigger and cRaF-S621 signals. The difference between the sys-  
163 tem state with and without the gene knockouts (encoded as a state displacement matrix)  
164 was decomposed using Singular Value Decomposition (SVD). A panel of twenty param-  
165 eter sets was sampled, and the average displacement matrix was decomposed. The  
166 first four modes described >99% of the gene knockout variance, with the most important  
167 components of these modes being the PU.1 and AP1 proteins, and to a much lesser ex-  
168 tent Gfi1 and C/EBPa (Fig. 6A). To better understand which connections involving the  
169 PU.1 and AP1 proteins were important, we simulated the pairwise deletion of interac-  
170 tions between these proteins and their respective regulatory targets. SVD decomposition  
171 of the state displacement matrix assembled from the pairwise deletion of interactions,  
172 suggested the first five modes accounted for >99% of the variance resulting from dele-  
173 tion of the interactions. The most sensitive interactions for the PU.1 protein involved the  
174 C/EBPa-dependent regulation of P47Phox expression, and to a lesser extent AP1 and

<sup>175</sup> EGR1 expression (Fig. 6B). On the other other, the most sensitive connections for AP1  
<sup>176</sup> involved the C/EBPa-dependent regulation of p21 expression, and the mutual activation  
<sup>177</sup> of PU.1 and AP1 expression. Taken together, these results suggested that the PU.1 and  
<sup>178</sup> AP1 proteins acted as important self-reinforcing regulators for both the signal integration  
<sup>179</sup> and phenotype modules. The analysis suggested that the PU.1 signaling axis promoted  
<sup>180</sup> the formation of the neutrophil NADPH oxidase (through p47Phox), while AP1 was re-  
<sup>181</sup> sponsible for cell cycle arrest (through p21). However, this analysis did not give insight  
<sup>182</sup> into which upstream components of the signal initiation module were important. Toward  
<sup>183</sup> this question, we explored the composition and regulation of the signalsome complex by  
<sup>184</sup> experimentally interrogating a panel of possible Raf interaction partners.

<sup>185</sup> The composition of the signalsome, and the kinase ultimately responsible for medi-  
<sup>186</sup> ating ATRA-induced Raf activation is currently unknown. To explore this question, we  
<sup>187</sup> conducted immunoprecipitation and subsequent Western blotting to identify physical in-  
<sup>188</sup> teractions between Raf and 19 putative interaction partners. A panel of 19 possible Raf  
<sup>189</sup> interaction partners (kinases, GTPases, scaffolding proteins etc) was constructed based  
<sup>190</sup> upon known signaling pathways. We did not consider the most likely binding partner, the  
<sup>191</sup> small GTPase RAS, as previous studies have ruled it out in MAPK activation in HL-60 cells  
<sup>192</sup> (20, 27). Total Raf was used as a bait protein for the immunoprecipitation studies. Interro-  
<sup>193</sup> gation of the Raf interactome suggested Vav1 was involved with ATRA-induced initiation  
<sup>194</sup> of MAPK activity (Fig. 7). Western blot analysis using total Raf and pS621 Raf specific  
<sup>195</sup> antibodies confirmed the presence of the bait protein, total and phosphorylated forms, in  
<sup>196</sup> the immunoprecipitate (Fig. 7A). Of the 19 proteins sampled, Vav1, Src, CK2, Akt, and  
<sup>197</sup> 14-3-3 precipitated with Raf, suggesting a direct physical interaction was possible. How-  
<sup>198</sup> ever, only the associations between Raf and Vav1 and Raf and Src were ATRA-inducible  
<sup>199</sup> (Fig. 7). Furthermore, the Vav1 and Src associations were correlated with pS621 Raf  
<sup>200</sup> abundance in the precipitate. Others proteins e.g., CK2, Akt and 14-3-3, generally bound

201 Raf regardless of phosphorylation status or ATRA treatment. The remaining 14 proteins  
202 were expressed in whole cell lysate (Fig. 7B), but were not detectable in the precipitate  
203 of Raf IP. Treatment with the Raf kinase inhibitor GW5074 following ATRA exposure re-  
204 duced the association of both Vav1 with Raf and Src with Raf (Fig. 7), although the signal  
205 intensity for Src was notably weak. However, GW5074 did not influence the association  
206 of CK2 or 14-3-3 with Raf, further demonstrating their independence from Raf phospho-  
207 rylation. Interestingly, the Raf-Akt interaction qualitatively increased following treatment  
208 with GW5074; however, it remained unaffected by treatment with ATRA. Src family ki-  
209 nases are known to be important in myeloid differentiation (28) and their role in HL-60  
210 differentiation has been investigated elsewhere (11). Given the existing work and variable  
211 reproducibility in the context of the Raf immunoprecipitate, we did not investigate the role  
212 of Src further in this study. Taken together, the immunoprecipitation and GW5074 results  
213 implicated Vav1 association to be correlated with Raf activation following ATRA-treatment.  
214 Previous studies demonstrated that a Vav1-Slp76-Cbl-CD38 complex plays an important  
215 role in ATRA-induced MAPK activation and differentiation of HL-60 cells (13). Here we  
216 did not observe direct interaction of Raf with Cbl or Slp76; however, this complex could  
217 be involved upstream. Next, we considered the effect of the Raf kinase inhibitor GW5074  
218 on functional markers of ATRA-induced growth arrest and differentiation.

219 Inhibition of Raf kinase activity modulated MAPK activation and differentiation mark-  
220 ers following ATRA exposure (Fig. 7D-F). ATRA treatment alone statistically significantly  
221 increased the G1/G0 percentage over the untreated control, while GW5074 alone had a  
222 negligible effect on the cell cycle distribution (Fig. 7D). Surprisingly, the combination of  
223 GW5074 and ATRA statistically significantly increased the G1/G0 population ( $82 \pm 1\%$ )  
224 compared with ATRA alone ( $61 \pm 0.5\%$ ). Increased G1/G0 arrest following the combined  
225 treatment with GW5074 and ATRA was unexpected, as the combination of ATRA and the  
226 MEK inhibitor (PD98059) has been shown previously to decrease ATRA-induced growth

arrest (8). However, growth arrest is not the sole indication of functional differentiation. Expression of the cell surface marker CD11b has also been shown to coincide with HL-60 cells myeloid differentiation (29). We measured CD11b expression, for the various treatment groups, using immuno-fluorescence flow cytometry 48 hr post-treatment. As with G1/G0 arrest, ATRA alone increased CD11b expression over the untreated control, while GW5074 further enhanced ATRA-induced CD11b expression (Fig. 7E). GW5074 alone had no statistically significant effect on CD11b expression, compared with the untreated control. Lastly, the inducible reactive oxygen species (ROS) response was used as a functional marker of differentiated neutrophils (16). We measured the ROS response induced by the phorbol ester 12-O-tetradecanoylphorbol-13-acetate (TPA) using flow cytometry. Untreated cells showed no discernible TPA response, with only  $7.0 \pm 3.0\%$  ROS induction (Fig. 7F). Cells treated with ATRA had a significantly increased TPA response,  $53 \pm 7\%$  ROS induction 48 hr post-treatment. Treatment with both ATRA and GW5074 statistically significantly reduced ROS induction ( $22 \pm 0.6\%$ ) compared to ATRA alone. Interestingly, Western blot analysis did not detect a GW5074 effect on ATRA-induced expression of p47phox, a required upstream component of the ROS response (Fig. 7F, bottom). Thus, the inhibitory effect of GW5074 on inducible ROS might occur downstream of p47phox expression. However, the ROS producing complex is MAPK dependent, therefore it is also possible that GW5074 inhibited ROS production by interfering with MAPK activation (in which case the p47Phox marker might not accurately reflect phenotypic conversion and differentiation).

248 **Discussion**

249 In this study, we presented an effective model of ATRA-inducible differentiation of HL-60  
250 cells. The model consisted of three modules: a signal initiation module that sensed and  
251 transformed the ATRA signal into activated cRaf-pS621 and the ATRA-RXR/RAR (Trig-  
252 ger) signals; a signal integration module that controlled the expression of upstream tran-  
253 scription factors given cRaf-pS621 and activated Trigger signals; and a phenotype mod-  
254 ule which encoded the expression of functional differentiation markers from the ATRA-  
255 inducible transcription factors. The model described the transcription and translation of  
256 genes in each module, and signaling events in each module in a growing population of  
257 HL-60 cells. Model parameters were largely taken from literature, however, unknown  
258 coefficients were estimated from protein measurements in HL-60 cells following ATRA  
259 exposure. Despite its simplicity, the effective model captured key features of the ATRA  
260 induced differentiation such as sustained MAPK activation, and bistability with respect  
261 to ATRA exposure. The model also described the expression of upstream transcription  
262 factors which regulated the expression of differentiation markers. Lastly, analysis of the  
263 response of the model to perturbations identified PU.1 and AP1 as master regulators of  
264 ATRA-induced differentiation. We also reported a new ATRA-inducible component of the  
265 signalsome, Vav1. Vav1 is a guanine nucleotide exchange factor for Rho family GTPases  
266 that activate pathways leading to actin cytoskeletal rearrangements and transcriptional al-  
267 terations (30). The Vav1/Raf association correlated with Raf activity, was ATRA-inducible  
268 and decreased after treatment with the Raf inhibitor GW5074.

269 Naturally occurring cell fate decisions often incorporate reinforcing feedback and bista-  
270 bility (31, 32). One of the most well studied cell fate circuits is the Mos mitogen-activated  
271 protein kinase cascade in *Xenopus* oocytes. This cascade is activated when oocytes are  
272 induced by the steroid hormone progesterone (33). The MEK-dependent activation of  
273 p42 MAPK stimulates the accumulation of the Mos oncprotein, which in turn activates

274 MEK, thereby closing the feedback loop. This is similar to the signal initiation module  
275 presented here; ATRA drives signalsome formation, which activates MAPK, which in turn  
276 leads to more signalsome activation. Thus, while HL-60 and *Xenopus* oocytes are vastly  
277 different biological models, their cell fate programs share a similar architectural feature.  
278 Reinforcing feedback and bistability has also been implicated in hematopoietic cell fate  
279 determination. Laslo et al showed that the counter antagonistic repressors, Gfi-1 and  
280 Egr-1/2 (whose expression is tuned by PU.1 and C/EBPa), encodes a bistable switch that  
281 results in a macrophage, neutrophil or a mixed lineage population depending upon PU.1  
282 and C/EBPa expression (32). The current model contained the Gfi-1 and Egr-1/2 agonis-  
283 tic switch; however, its significance was unclear for HL-60 cells. The expression of Gfi-1,  
284 Egr-1/2, C/EBPa and PU.1 was not consistent with the canonical lineage pattern expected  
285 from literature. For example, Egr-1/2 expression (associated with a macrophage lineage)  
286 increased, while Gfi-1 expression (associated with a neutrophil lineage) remained con-  
287 stant following ATRA exposure. Literature evidence in nonmalignant myelomonocytic fate  
288 selection has shown that Gfi-1 and EGR-1/2 promote granulocytic and monocytic differ-  
289 entiation, respectively (32). Thus, HL-60 cells, which are a less mature cancer cell line,  
290 exhibited a non-canonical expression pattern. Other unrelated cell fate decisions such  
291 as programmed cell death have also been suggested to be bistable (34). Still more bio-  
292 chemical networks important to human health, for example the human coagulation or  
293 complement cascades, also feature strong positive feedback elements (35). Thus, while  
294 reinforcing feedback is often undesirable in human engineered systems, it is at the core  
295 of a diverse variety of cell fate programs and other networks important to human health.

296 Analysis of the signal integration and phenotype modules suggested that PU.1 and  
297 AP1 regulated distinct phenotypic axes following ATRA exposure. The PU.1 transcription  
298 factor, a member of the ets transcription factor family, is a well known regulatory protein  
299 in granulocyte and monocyte development (36). The relative level of PU.1 and C/EBPa

300 regulates macrophage versus neutrophil cell fate decisions in granulocytic macrophage  
301 progenitor cells (37).

302 Immunoprecipitation studies identified a limited number of ATRA-dependent and -  
303 independent Raf interaction partners. While we were unable to detect the association  
304 of Raf with common kinases and GTPases such as PKC, PKA, p38, Rac and Rho, we  
305 did establish potential interactions between Raf and key partners such as Vav1, Src, Akt,  
306 CK2 and 14-3-3. All of these partners are known to be associated with Raf activation  
307 or function. Src is known to bind Raf through an SH2 domain, and this association has  
308 been shown to be dependent of the serine phosphorylation of Raf (38). Thus, an ATRA in-  
309 ductible Src/Raf association may be a result of ATRA-induced Raf phosphorylation at S259  
310 or S621. We also identified an interaction between Raf and the Ser/Thr kinases Akt and  
311 CK2. Akt can phosphorylate Raf at S259, as demonstrated by studies in a human breast  
312 cancer line (39). CK2 can also phosphorylate Raf, although the literature has traditionally  
313 focused on S338 and not S621 or S259(40). However, neither of these kinase interactions  
314 were ATRA-inducible, suggesting their association with Raf alone was not associated with  
315 ATRA-induced Raf phosphorylation. The adapter protein 14-3-3 was also constitutively  
316 associated with Raf. The interaction between Raf and 14-3-3 has been associated with  
317 both S621 and S259 phosphorylation and activity (41). Additionally, the association of  
318 Raf with 14-3-3 not only stabilized S621 phosphorylation, but also reversed the S621  
319 phosphorylation from inhibitory to activating (42). Finally, we found that Vav1/Raf associ-  
320 ation correlated with Raf activity, was ATRA-inducible and decreased after treatment with  
321 GW5074. The presence of Vav1 in Raf/Grb2 complexes has been shown to correlate with  
322 increased Raf activity in mast cells (43). Furthermore, studies on Vav1 knockout mice  
323 demonstrated that the loss of Vav1 resulted in deficiencies of ERK signaling for both T-  
324 cells as well as neutrophils (44, 45). Interestingly, while an integrin ligand-induced ROS  
325 response was blocked in Vav1 knockout neutrophils, TPA was able to bypass the Vav1

326 requirement and stimulate both ERK phosphorylation and ROS induction (45). In this  
327 study, the TPA-induced ROS response was dependent upon Raf kinase activity, and was  
328 mitigated by the addition of GW5074. It is possible that Vav1 is downstream of various  
329 integrin receptors but upstream of Raf in terms of inducible ROS responses. Vav1 has  
330 also been shown to associate with a Cbl-Slp76-CD38 complex in an ATRA-dependent  
331 manner; furthermore, transfection of HL-60 cells with Cbl mutants that fail to bind CD38,  
332 yet still bind Slp76 and Vav1, prevents ATRA-induced MAPK activation (13). The literature  
333 suggest a variety of possible receptor-signaling pathways, which involve Vav1, for MAPK  
334 activation; moreover, given the ATRA-inducible association Vav1 may play a direct role in  
335 Raf activation.

336 We hypothesized that Vav1 is a member of an ATRA-inducible complex which propels  
337 sustained MAPK activation, arrest and differentiation. Initially, ATRA-induced Vav1 ex-  
338 pression drives increased association between Vav1 and Raf. This increased interaction  
339 facilitates phosphorylation and activation of Raf by pre-bound Akt and/or CK2 at S621  
340 or perhaps S259. Constitutively bound 14-3-3 may also stabilize the S621 phosphory-  
341 lation, modulate the activity and/or up-regulate autophosphorylation. Activated Raf can  
342 then drive ERK activation, which in turn closes the positive feedback loop by activating  
343 Raf transcription factors e.g., Sp1 and/or STAT1 (46–49). We tested this working hy-  
344 pothesis using mathematical modeling. The model recapitulated both ATRA time-course  
345 data as well as the GW5074 inhibitor effects. This suggested the proposed Raf-Vav1  
346 architecture was at least consistent with the experimental studies. Further, analysis of  
347 the Raf-Vav1 model identified bistability in ppERK levels. Thus, two possible MAPK ac-  
348 tivation branches were possible for experimentally testable ATRA values. The analysis  
349 also suggested the ATRA-induced Raf-Vav1 architecture could be locked into a sustained  
350 signaling mode (high ppERK) even in the absence of a ATRA signal. This locked-in prop-  
351 erty could give rise to an ATRA-induction memory. We validated the treatment memory

352 property predicted by the Raf-Vav1 circuit experimentally using ATRA-washout experiments.  
353 ERK phosphorylation levels remained high for more than 96 hr after ATRA was  
354 removed. Previous studies demonstrated that HL-60 cells possessed an inheritable mem-  
355 ory of ATRA stimulus (50). Although the active state was self-sustaining, the inactive state  
356 demonstrated considerable robustness to perturbation. For example, we found that 50x  
357 overexpression of Raf was required to reliably lock MAPK into the activated state, while  
358 small perturbations had almost no effect on ppERK levels over the entire ensemble. CD38  
359 expression correlated with the ppERK, suggesting its involvement in the signaling com-  
360 plex. Our computational and experimental results showed that positive feedback, through  
361 ERK-dependent Raf expression, could sustain MAPK signaling through many division cy-  
362 cles. Such molecular mechanisms could underly aspects of cellular memory associated  
363 to consecutive ATRA treatments.

364 There were several issues that can be explored further with the effective ATRA differ-  
365 entiation model. First, there was likely missing connectivity in the effective differentiation  
366 circuit. Decreasing BLR1 expression with simultaneously sustained cRaf-pS261 activa-  
367 tion was not captured by the current network architecture. This suggested that signal-  
368 some, once activated, had a long lifetime as decreased BLR1 expression did not impact  
369 cRaf-pS261 abundance. We could model this by separating signalsome formation into an  
370 inactive precursor pool that is transformed to a long-lived activated signalsome by MAPK  
371 activation. We should also explore adding additional downstream biological modules to  
372 this skeleton model, for example the upregulation of reactive oxygen markers such as  
373 p47Phox or cell cycle arrest components to capture the switch from an actively prolifer-  
374 ating population to a population in G0-arrest. Next, the choice of max/min integration  
375 rules or the particular form of the transfer functions could also be explored. Integration  
376 rules other than max/min could be used, such as the mean or the product, assuming the  
377 range of the transfer functions is always  $f \in [0, 1]$ . Alternative integration rules might

<sup>378</sup> have different properties which could influence model identification or performance. For  
<sup>379</sup> example, a mean integration rule would be differentiable, allowing derivative-based opti-  
<sup>380</sup> mization approaches to be used. The form of the transfer function could also be explored.  
<sup>381</sup> We choose hill-like functions because of their prominence in the systems and synthetic  
<sup>382</sup> biology community. However, many other transfer functions are possible.

383 **Materials and Methods**

384 *Effective gene expression model equations.* We decomposed the ATRA-induced differ-  
 385 entiation program into three modules; a signal initiation module that sensed and trans-  
 386 formed the ATRA signal into activated cRaf-pS621 and the ATRA-RXR/RAR (activated  
 387 Trigger) signals; a signal integration module that controlled the expression of upstream  
 388 transcription factors given cRaf-pS621 and activated Trigger signals; and a phenotype  
 389 module which encoded the expression of functional differentiation markers from the ATRA-  
 390 inducible transcription factors. The output of the signal initiation module was the input to  
 391 the gene expression model. For each gene  $j = 1, 2, \dots, \mathcal{G}$ , we modeled both the mRNA  
 392 ( $m_j$ ), protein ( $p_j$ ) and signaling species abundance:

$$\frac{dm_j}{dt} = r_{T,j} - (\mu + \theta_{m,j}) m_j + \lambda_j \quad (1)$$

$$\frac{dp_j}{dt} = r_{X,j} - (\mu + \theta_{p,j}) p_j \quad (2)$$

$$g(p_1, \dots, p_{\mathcal{G}}, \kappa) = 0 \quad (3)$$

393 The terms  $r_{T,j}$  and  $r_{X,j}$  denote the specific rates of transcription, and translation while  
 394 the terms  $\theta_{m,j}$  and  $\theta_{p,j}$  denote first-order degradation constants for mRNA and protein,  
 395 respectively. The specific transcription rate  $r_{T,j}$  was modeled as the product of a kinetic  
 396 term  $\bar{r}_{T,j}$  and a control term  $u_j$  which described how the abundance of transcription fac-  
 397 tors, or other regulators influenced the expression of gene  $j$ . The kinetic transcription  
 398 term  $\bar{r}_{T,j}$  was modeled as:

$$\bar{r}_{T,j} = V_T^{max} \left( \frac{L_{T,o}}{L_{T,j}} \right) \left( \frac{G_j}{K_T + G_j} \right) \quad (4)$$

399 where the maximum gene expression rate  $V_T^{max}$  was defined as the product of a char-  
 400 acteristic transcription rate constant ( $k_T$ ) and the abundance of RNA polymerase ( $R_1$ ),

401  $V_T^{max} = k_T(R_1)$ . The  $(L_{T,o}/L_{T,j})$  term denotes the ratio of transcription read lengths;  $L_{T,o}$   
 402 represents a characteristic gene length, while  $L_{T,j}$  denotes the length of gene  $j$ . Thus,  
 403 the ratio  $(L_{T,o}/L_{T,j})$  is a gene specific correction to the characteristic transcription rate  
 404  $V_T^{max}$ . The degradation rate constants were defined as  $\theta_{m,j}$  and  $\theta_{p,j}$  denote characteristic  
 405 degradation constants for mRNA and protein, respectively. Lastly, the  $\lambda_j$  term denotes the  
 406 constitutive rate of expression of gene  $j$ .

407 The gene expression control term  $0 \leq u_j \leq 1$  depended upon the combination of fac-  
 408 tors which influenced the expression of gene  $j$ . If the expression of gene  $j$  was influenced  
 409 by  $1, \dots, m$  factors, we modeled this relationship as  $u_j = \mathcal{I}_j(f_{1j}(\cdot), \dots, f_{mj}(\cdot))$  where  
 410  $0 \leq f_{ij}(\cdot) \leq 1$  denotes a regulatory transfer function quantifying the influence of factor  $i$   
 411 on the expression of gene  $j$ , and  $\mathcal{I}_j(\cdot)$  denotes an integration rule which combines the  
 412 individual regulatory inputs for gene  $j$  into a single control term. In this study, the integra-  
 413 tion rule governing gene expression was the weighted fraction of promoter configurations  
 414 that resulted in gene expression (51):

$$u_j = \frac{W_{R_{1,j}} + \sum_n W_{nj} f_{nj}}{1 + W_{R_{1,j}} + \sum_d W_{dj} f_{dj}} \quad (5)$$

415 The numerator, the weighted sum (with weights  $W_{nj}$ ) of promoter configurations leading to  
 416 gene expression, was normalized by all possible promoter configurations. The likelihood  
 417 of each configuration was quantified by the transfer function  $f_{nj}$  (which we modeled using  
 418 hill like functions), while the lead term in the numerator  $W_{R_{1,j}}$  denotes the weight of con-  
 419 stitutive expression for gene  $j$ . Given this formulation, the rate of constitutive expression  
 420 was then given by:

$$\lambda_j = \bar{r}_{T,j} \left( \frac{W_{R_{1,j}}}{1 + W_{R_{1,j}}} \right) \quad (6)$$

421 If a gene expression process had no modifying factors,  $u_j = 1$ . Lastly, the specific trans-

422 lation rate was modeled as:

$$r_{X,j} = V_X^{\max} \left( \frac{L_{X,o}}{L_{X,j}} \right) \left( \frac{m_j}{K_X + m_j} \right) \quad (7)$$

423 where  $V_X^{\max}$  denotes a characteristic maximum translation rate estimated from literature,  
424 and  $K_X$  denotes a translation saturation constant. The characteristic maximum translation  
425 rate was defined as the product of a characteristic translation rate constant ( $k_X$ ) and  
426 the Ribosome abundance ( $R_2$ ),  $V_X^{\max} = k_X (R_2)$ . As was the case for transcription, we  
427 corrected the characteristic translation rate by the ratio of the length of a characteristic  
428 transcription normalized by the length of transcript  $j$ .

429 *Signaling model equations.* The signal initiation, and integration modules required the  
430 abundance of cRaf-pS621 and ATRA-RXR/RAR (activated Trigger) as inputs. However,  
431 our base model described only the abundance of inactive proteins e.g., cRaf or RXR/RAR  
432 but not the activated forms. To address this issue, we estimated pseudo steady state  
433 approximations for the abundance of cRaf-pS621 and activated Trigger (shown generally  
434 as Eq (3)). The abundance of activated trigger ( $x_{a,1}$ ) was estimated directly from the  
435 RXR/RAR abundance ( $x_{u,1}$ ):

$$x_{a,1} \sim x_{u,1} \left( \frac{\alpha \cdot \text{ATRA}}{1 + \alpha \cdot \text{ATRA}} \right) \quad (8)$$

436 where  $\alpha$  denotes a gain parameter;  $\alpha = 0.0$  if ATRA is less than a threshold, and  $\alpha = 0.1$   
437 if ATRA is greater than the differentiation threshold. The abundance of cRaf-pS621 was  
438 estimated by making the pseudo steady state approximation on the cRaf-pS621 balance.  
439 The abundance of an activated signaling species  $i$  was given by:

$$\frac{dx_i}{dt} = r_{+,i}(\mathbf{x}, \mathbf{k}) - (\mu + k_{d,i}) x_i \quad i = 1, \dots, \mathcal{M} \quad (9)$$

440 The quantity  $x_i$  denotes concentration of signaling species  $i$ , while  $\mathcal{R}$  and  $\mathcal{M}$  denote  
 441 the number of signaling reactions and signaling species in the model, respectively. The  
 442 term  $r_{+,i}(\mathbf{x}, \mathbf{k})$  denotes the rate of generation of activated species  $i$ , while  $\mu$  denotes  
 443 the specific growth rate, and  $k_{d,i}$  denotes the rate constant controlling the non-specific  
 444 degradation of  $x_i$ . We neglected deactivation reactions e.g., phosphatase activities. We  
 445 assumed that signaling processes were fast compared to gene expression; this allowed  
 446 us to approximate the signaling balance as:

$$x_i^* \simeq \frac{r_{+,i}(\mathbf{x}, \mathbf{k})}{(\mu + k_{d,i})} \quad i = 1, \dots, \mathcal{M} \quad (10)$$

447 The generation rate was written as the product of a kinetic term ( $\bar{r}_{+,i}$ ) and a control term  
 448 ( $v_i$ ). The control terms  $0 \leq v_j \leq 1$  depended upon the combination of factors which in-  
 449 fluenced rate process  $j$ . If rate  $j$  was influenced by  $1, \dots, m$  factors, we modeled this  
 450 relationship as  $v_j = \mathcal{I}_j(f_{1j}(\cdot), \dots, f_{mj}(\cdot))$  where  $0 \leq f_{ij}(\cdot) \leq 1$  denotes a regulatory  
 451 transfer function quantifying the influence of factor  $i$  on rate  $j$ . The function  $\mathcal{I}_j(\cdot)$  is an  
 452 integration rule which maps the output of regulatory transfer functions into a control vari-  
 453 able. In this study, we used  $\mathcal{I}_j \in \{\min, \max\}$  and hill transfer functions (52). If a process  
 454 had no modifying factors,  $v_j = 1$ . The kinetic rate of cRaf-pS621 generation  $\bar{r}_{+,cRaf}$  was  
 455 modeled as:

$$\bar{r}_{+,cRaf} = k_{+,cRaf} x_s \left( \frac{x_{cRaf}}{K_{+,cRaf} + x_{cRaf}} \right) \quad (11)$$

456 where  $x_s$  denotes the signalsome abundance, and  $K_{+,cRaf}$  denotes a saturation constant  
 457 governing cRaf-pS621 formation. The formation of cRaf-pS621 was regulated by only a  
 458 single factor, the abundance of MAPK inhibitor, thus  $v_{+,cRaf}$  took the form:

$$v_{+,cRaf} = \left( 1 - \frac{I}{K_D + I} \right) \quad (12)$$

459 where  $I$  denotes the abundance of the MAPK inhibitor, and  $K_D$  denotes the inhibitor  
460 affinity.

461 *Estimation of gene expression model parameters.* We estimated parameters appearing  
462 in the mRNA and protein balances, the abundance of polymerases and ribosomes, tran-  
463 scription and translation rates, the half-life of a typical mRNA and protein, and typical  
464 values for the copies per cell of RNA polymerase and ribosomes from literature (Table 2).  
465 The saturation constants  $K_X$  and  $K_T$  were adjusted so that gene expression and trans-  
466 lation resulted in gene products on a biologically realistic concentration scale. Lastly, we  
467 calculated the concentration for gene  $G_j$  by assuming, on average, that a cell had two  
468 copies of each gene at any given time. Thus, the bulk of our gene expression model pa-  
469 rameters were based directly upon literature values, and were not adjusted during model  
470 identification. However, the remaining parameters, e.g., the  $W_{ij}$  appearing in the gene  
471 expression control laws, or parameters appearing in the transfer functions  $f_{dij}$ , were esti-  
472 mated from the protein expression and signaling data sets discussed here.

473 Signaling and gene expression model parameters were estimated by minimizing the  
474 squared difference between simulations and experimental protein data set  $j$ . We mea-  
475 sured the squared difference in the scale, fold change and shape for protein  $j$ :

$$E_j(\mathbf{k}) = \left( \mathcal{M}_j(t_-) - \hat{y}_j(t_-, \mathbf{k}) \right)^2 + \sum_{i=1}^{\mathcal{T}_j} \left( \hat{\mathcal{M}}_{ij} - \hat{y}_{ij}(\mathbf{k}) \right)^2 + \sum_{i=1}^{\mathcal{T}_j} \left( \mathcal{M}'_{ij} - y'_{ij}(\mathbf{k}) \right)^2 \quad (13)$$

476 The first term in Eqn. (13) quantified the initial *scale* error, directly before the addition  
477 of ATRA. In this case,  $\mathcal{M}_j(t_-)$  (the approximate concentration of protein  $j$  before the  
478 addition of ATRA) was estimated from literature. This term was required because the  
479 protein measurements were reported as the fold-change; thus, the data was normalized  
480 by a control value measured before the addition of ATRA. However, the model operated on  
481 a physical scale. The first term allowed the model to capture physically realistic changes

following ATRA addition. The second term quantified the difference in the *fold-change* of protein  $j$  as a function of time. The terms  $\hat{\mathcal{M}}_{ij}$  and  $\hat{y}_{ij}$  denote the scaled experimental observations and simulation outputs (fold-change; protein normalized by control value directly before ATRA addition) at time  $i$  from protein  $j$ , where  $T_j$  denoted the number of time points for data set  $j$ . Lastly, the third term of the objective function measured the difference in the *shape* of the measured and simulated protein levels. The scaled value  $0 \leq \mathcal{M}'_{ij} \leq 1$  was given by:

$$\hat{\mathcal{M}}_{ij} = \left( \mathcal{M}_{ij} - \min_i \mathcal{M}_{ij} \right) / \left( \max_i \mathcal{M}_{ij} - \min_i \mathcal{M}_{ij} \right) \quad (14)$$

where  $\mathcal{M}'_{ij} = 0$  and  $\mathcal{M}'_{ij} = 1$  describe the lowest (highest) intensity bands. A similar scaling was used for the simulation output. We minimized the total model residual  $\sum_j E_j$  using a heuristic direct-search optimization procedure, subject to box constraints on the parameter values, starting from a random initial parameter guess. Each downhill step was archived and used for ensemble calculations. The optimization procedure (a covariance matrix adaptation evolution strategy) has been reported previously (53).

*Estimation of an effective cell cycle arrest model.* We formulated an effective N-order polynomial model of the fraction of cells undergoing ATRA-induced cell cycle arrest at time  $t$ ,  $\hat{\mathcal{A}}(t)$ , as:

$$\hat{\mathcal{A}}(t) \simeq a_0 + \sum_{i=1}^{N-1} a_i \phi_i(\mathbf{p}(t), t) \quad (15)$$

where  $a_i$  were unknown parameters, and  $\phi_i(\mathbf{p}(t), t)$  denotes a basis function. The basis functions were dependent upon the system state; in this study, we assumed  $N = 4$  and basis functions of the form:

$$\phi_i(\mathbf{p}(t), t) = \left( \frac{t}{T} + \frac{p21}{E2F} \Big|_t \right)^{(i-1)} \quad (16)$$

501 The parameters  $a_0, \dots, a_3$  were estimated directly from cell-cycle measurements (biologi-  
502 cal replicates) using least-squares.

503 *Availability of model code.* The signaling and gene expression model equations, and the  
504 parameter estimation procedure, were implemented in the Julia programming language.  
505 The model equations were solved using the ODE23s routine of the ODE package (54). The  
506 model code and parameter ensemble is freely available under an MIT software license  
507 and can be downloaded from <http://www.varnerlab.org>.

508 *Cell culture and treatment* Human myeloblastic leukemia cells (HL-60 cells) were grown  
509 in a humidified atmosphere of 5% CO<sub>2</sub> at 37°C and maintained in RPMI 1640 from Gibco  
510 (Carlsbad, CA) supplemented with 5% heat inactivated fetal bovine serum from Hyclone  
511 (Logan, UT) and 1× antibiotic/antimicotic (Gibco, Carlsbad, CA). Cells were cultured in  
512 constant exponential growth (55). Experimental cultures were initiated at  $0.1 \times 10^6$  cells/mL  
513 24 hr prior to ATRA treatment; if indicated, cells were also treated with GW5074 (2 $\mu$ M) 18  
514 hr before ATRA treatment. For the cell culture washout experiments, cells were treated  
515 with ATRA for 24 hr, washed 3x with prewarmed serum supplemented culture medium  
516 to remove ATRA, and reseeded in ATRA-free media as described. Western blot analysis  
517 was performed at incremental time points after removal of ATRA.

518 *Chemicals* All-Trans Retinoic Acid (ATRA) from Sigma-Aldrich (St. Louis, MO) was dis-  
519 solved in 100% ethanol with a stock concentration of 5mM, and used at a final concen-  
520 tration of 1 $\mu$ M (unless otherwise noted). The cRaf inhibitor GW5074 from Sigma-Aldrich  
521 (St. Louis, MO) was dissolved in DMSO with a stock concentration of 10mM, and used  
522 at a final concentration of 2 $\mu$ M. HL-60 cells were treated with 2 $\mu$ M GW5074 with or with-  
523 out ATRA (1 $\mu$ M) at 0 hr. This GW5074 dosage had a negligible effect on the cell cycle  
524 distribution, compared to ATRA treatment alone.

525 *Immunoprecipitation and western blotting* Approximately  $1.2 \times 10^7$  cells were lysed using  
526  $400\mu\text{L}$  of M-Per lysis buffer from Thermo Scientific (Waltham, MA). Lysates were cleared  
527 by centrifugation at  $16,950 \times g$  in a micro-centrifuge for 20 min at  $4^\circ\text{C}$ . Lysates were  
528 pre-cleared using  $100\mu\text{L}$  protein A/G Plus agarose beads from Santa Cruz Biotechnology  
529 (Santa Cruz, CA) by inverting overnight at  $4^\circ\text{C}$ . Beads were cleared by centrifugation and  
530 total protein concentration was determined by a BCA assay (Thermo Scientific, Waltham,  
531 MA). Immunoprecipitations were setup by bringing lysate to a concentration of 1g/L in a  
532 total volume of  $300\mu\text{L}$  (M-Per buffer was used for dilution). The anti-Raf antibody was  
533 added at  $3\mu\text{L}$ . A negative control with no bait protein was also used to exclude the di-  
534 rect interaction of proteins with the A/G beads. After 1 hr of inversion at  $4^\circ\text{C}$ ,  $20\mu\text{L}$  of  
535 agarose beads was added and samples were left to invert overnight at  $4^\circ\text{C}$ . Samples  
536 were then washed three times with M-Per buffer by centrifugation. Finally proteins were  
537 eluted from agarose beads using a laemmli loading buffer. Eluted proteins were resolved  
538 by SDS-PAGE and Western blotting. Total lysate samples were normalized by total protein  
539 concentration ( $20\mu\text{g}$  per sample) and resolved by SDS-PAGE and Western blotting. Sec-  
540 ondary HRP bound antibody was used for visualization. All antibodies were purchased  
541 from Cell Signaling (Boston, MA) with the exception of  $\alpha$ -p621 Raf which was purchased  
542 from Biosource/Invitrogen (Carlsbad, CA), and  $\alpha$ -CK2 from BD Biosciences (San Jose,  
543 CA).

544 *Morphology assessment* Untreated and ATRA-treated HL-60 cells were collected after  
545 72 hr and cytocentrifuged for 3 min at 700 rpm onto glass slides. Slides were air-dried  
546 and stained with Wright's stain. Slide images were captured at 40X (Leica DM LB 100T  
547 microscope, Leica Microsystems).

548 **Competing interests**

549 The authors declare that they have no competing interests.

550 **Author's contributions**

551 J.V and A.Y directed the study. R.T, H.J, R.B and J.C conducted the cell culture measure-  
552 ments. J.V, R.B, W.D, K.R and A.S developed the reduced order HL-60 models and the  
553 parameter ensemble. W.D and J.V analyzed the model ensemble, and generated figures  
554 for the manuscript. The manuscript was prepared and edited for publication by W.D, A.Y  
555 and J.V.

556 **Acknowledgements**

557 We gratefully acknowledge the suggestions from the anonymous reviewers to improve  
558 this manuscript.

559 **Funding**

560 We acknowledge the financial support to J.V. by the National Science Foundation CA-  
561 REER (CBET-0846876) for the support of R.T. and H.J. In addition, we acknowledge  
562 support to A.Y. from the National Institutes of Health (CA 30555, CA152870) and a grant  
563 from New York State Stem Cell Science. Lastly, we acknowledge the financial support to  
564 J.V. and A.Y. from the National Cancer Institute (#U54 CA143876). The content is solely  
565 the responsibility of the authors and does not necessarily represent the official views of  
566 the National Cancer Institute or the National Institutes of Health.

567 **References**

- 568 1. Bushue N, Wan YJY (2010) Retinoid pathway and cancer therapeutics. *Adv Drug  
569 Deliv Rev* 62: 1285-98.
- 570 2. Tang XH, Gudas LJ (2011) Retinoids, retinoic acid receptors, and cancer. *Annu Rev  
571 Pathol* 6: 345-64.
- 572 3. Cheung FSG, Lovicu FJ, Reichardt JKV (2012) Current progress in using vitamin d  
573 and its analogs for cancer prevention and treatment. *Expert Rev Anticancer Ther*  
574 12: 811-37.
- 575 4. Nilsson B (1984) Probable in vivo induction of differentiation by retinoic acid of  
576 promyelocytes in acute promyelocytic leukaemia. *Br J Haematol* 57: 365-71.
- 577 5. Warrell RP Jr (1993) Retinoid resistance in acute promyelocytic leukemia: new  
578 mechanisms, strategies, and implications. *Blood* 82: 1949-53.
- 579 6. Freemantle SJ, Spinella MJ, Dmitrovsky E (2003) Retinoids in cancer therapy and  
580 chemoprevention: promise meets resistance. *Oncogene* 22: 7305-15.
- 581 7. Breitman TR, Selonick SE, Collins SJ (1980) Induction of differentiation of the hu-  
582 man promyelocytic leukemia cell line (HL-60) by retinoic acid. *Proc Natl Acad Sci U  
583 S A* 77: 2936–2940.
- 584 8. Yen A, Roberson MS, Varvayanis S, Lee AT (1998) Retinoic acid induced  
585 mitogen-activated protein (MAP)/extracellular signal-regulated kinase (ERK) kinase-  
586 dependent MAP kinase activation needed to elicit HL-60 cell differentiation and  
587 growth arrest. *Cancer Res* 58: 3163–3172.
- 588 9. Hong HY, Varvayanis S, Yen A (2001) Retinoic acid causes MEK-dependent RAF  
589 phosphorylation through RARalpha plus RXR activation in HL-60 cells. *Differentia-  
590 tion* 68: 55–66.
- 591 10. Mangelsdorf DJ, Ong ES, Dyck JA, Evans RM (1990) Nuclear receptor that identifies  
592 a novel retinoic acid response pathway. *Nature* 345: 224–229.

- 593 11. Congleton J, MacDonald R, Yen A (2012) Src inhibitors, PP2 and dasatinib, increase  
594 retinoic acid-induced association of Lyn and c-Raf (S259) and enhance MAPK-  
595 dependent differentiation of myeloid leukemia cells. Leukemia 26: 1180-8.
- 596 12. Shen M, Bunaci R, Congleton J, Jensen H, Sayam L, et al. (2011) Interferon regu-  
597 latory factor-1 binds c-Cbl, enhances mitogen activated protein kinase signaling and  
598 promotes retinoic acid-induced differentiation of HL-60 human myelo-monoblastic  
599 leukemia cells. Leuk Lymphoma 52: 2372-9.
- 600 13. Shen M, Yen A (2009) c-Cbl tyrosine kinase-binding domain mutant G306E abol-  
601 ishes the interaction of c-Cbl with CD38 and fails to promote retinoic acid-induced  
602 cell differentiation and G0 arrest. J Biol Chem 284: 25664–25677.
- 603 14. Yen A, Varvayanis S, Smith J, Lamkin T (2006) Retinoic acid induces expression of  
604 SLP-76: expression with c-FMS enhances ERK activation and retinoic acid-induced  
605 differentiation/G0 arrest of HL-60 cells. Eur J Cell Biol 85: 117–132.
- 606 15. Marchisio M, Bertagnolo V, Colamussi ML, Capitani S, Neri LM (1998) Phos-  
607 phatidylinositol 3-kinase in HL-60 nuclei is bound to the nuclear matrix and increases  
608 during granulocytic differentiation. Biochem Biophys Res Commun 253: 346-51.
- 609 16. Congleton J, Jiang H, Malavasi F, Lin H, Yen A (2011) ATRA-induced HL-60 myeloid  
610 leukemia cell differentiation depends on the CD38 cytosolic tail needed for mem-  
611 brane localization, but CD38 enzymatic activity is unnecessary. Exp Cell Res 317:  
612 910–919.
- 613 17. Wang J, Yen A (2004) A novel retinoic acid-responsive element regulates retinoic  
614 acid induced BLR1 expression. Mol Cell Biol 24: 2423 - 2443.
- 615 18. Yen A (1990) HL-60 cells as a model of growth and differentiation: the significance  
616 of variant cells. Hematology Review 4: 5-46.
- 617 19. Yang T, Xiong Q, Enslen H, Davis R, Chow CW (2002) Phosphorylation of NFATc4  
618 by p38 mitogen-activated protein kinases. Mol Cell Biol 22: 3892–3904.

- 619 20. Wang J, Yen A (2008) A MAPK-positive Feedback Mechanism for BLR1 Signaling  
620 Propels Retinoic Acid-triggered Differentiation and Cell Cycle Arrest. *J Biol Chem*  
621 283: 4375–4386.
- 622 21. Tasseff R, Nayak S, Song S, Yen A, Varner J (2011) Modeling and analysis of retinoic  
623 acid induced differentiation of uncommitted precursor cells. *Integr Biol* 3: 578 - 591.
- 624 22. Jensen HA, Styskal LE, Tasseff R, Bunaciu RP, Congleton J, et al. (2013) The  
625 src-family kinase inhibitor pp2 rescues inducible differentiation events in emergent  
626 retinoic acid-resistant myeloblastic leukemia cells. *PLoS One* 8: e58621.
- 627 23. Jensen HA, Bunaciu RP, Ibabao CN, Myers R, Varner JD, et al. (2014) Retinoic acid  
628 therapy resistance progresses from unilineage to bilineage in hl-60 leukemic blasts.  
629 *PLoS One* 9: e98929.
- 630 24. Jensen HA, Bunaciu RP, Varner JD, Yen A (2015) Gw5074 and pp2 kinase inhibitors  
631 implicate nontraditional c-raf and lyn function as drivers of retinoic acid-induced mat-  
632 uration. *Cell Signal* 27: 1666-75.
- 633 25. Jensen HA, Yourish HB, Bunaciu RP, Varner JD, Yen A (2015) Induced myelomono-  
634 cytic differentiation in leukemia cells is accompanied by noncanonical transcription  
635 factor expression. *FEBS Open Bio* 5: 789-800.
- 636 26. Milo R, Jorgensen P, Moran U, Weber G, Springer M (2010) Bionumbers—the  
637 database of key numbers in molecular and cell biology. *Nucleic Acids Res* 38: D750-  
638 3.
- 639 27. Katagiri K, Hattori S, Nakamura S, Yamamoto T, Yoshida T, et al. (1994) Activation  
640 of ras and formation of gap complex during tpa-induced monocytic differentiation of  
641 hl-60 cells. *Blood* 84: 1780–1789.
- 642 28. Miranda MB, Johnson DE (2007) Signal transduction pathways that contribute to  
643 myeloid differentiation. *Leukemia* 21: 1363–1377.
- 644 29. Hickstein DD, Back AL, Collins SJ (1989) Regulation of expression of the cd11b and

- 645 cd18 subunits of the neutrophil adherence receptor during human myeloid differen-  
646 tiation. *J Biol Chem* 264: 21812–21817.
- 647 30. Hornstein I, Alcover A, Katzav S (2004) Vav proteins, masters of the world of cy-  
648 toskeleton organization. *Cell Signal* 16: 1-11.
- 649 31. Ferrell J (2002) Self-perpetuating states in signal transduction: positive feedback,  
650 double-negative feedback and bistability. *Curr Opin Cell Biol* 14: 140-8.
- 651 32. Laslo P, Spooner CJ, Warmflash A, Lancki DW, Lee HJ, et al. (2006) Multilineage  
652 transcriptional priming and determination of alternate hematopoietic cell fates. *Cell*  
653 126: 755-66.
- 654 33. Xiong W, Ferrell J (2003) A positive-feedback-based bistable 'memory module' that  
655 governs a cell fate decision. *Nature* 426: 460-5.
- 656 34. Bagci EZ, Vodovotz Y, Billiar TR, Ermentrout GB, Bahar I (2006) Bistability in apop-  
657 tosis: roles of bax, bcl-2, and mitochondrial permeability transition pores. *Biophys J*  
658 90: 1546-59.
- 659 35. Luan D, Zai M, Varner JD (2007) Computationally derived points of fragility of a  
660 human cascade are consistent with current therapeutic strategies. *PLoS Comput*  
661 *Biol* 3: e142.
- 662 36. Friedman AD (2007) Transcriptional control of granulocyte and monocyte develop-  
663 ment. *Oncogene* 26: 6816-28.
- 664 37. Dahl R, Walsh JC, Lancki D, Laslo P, Iyer SR, et al. (2003) Regulation of macrophage  
665 and neutrophil cell fates by the PU.1:C/EBPalpha ratio and granulocyte colony-  
666 stimulating factor. *Nat Immunol* 4: 1029-36.
- 667 38. Cleghon V, Morrison DK (1994) Raf-1 interacts with fyn and src in a non-  
668 phosphotyrosine-dependent manner. *J Biol Chem* 269: 17749–17755.
- 669 39. Zimmermann S, Moelling K (1999) Phosphorylation and regulation of raf by akt (pro-  
670 tein kinase b). *Science* 286: 1741–1744.

- 671 40. Ritt DA, Zhou M, Conrads TP, Veenstra TD, Copeland TD, et al. (2007) Ck2 is a  
672 component of the ksr1 scaffold complex that contributes to raf kinase activation.  
673 Curr Biol 17: 179–184.
- 674 41. Hekman M, Wiese S, Metz R, Albert S, Troppmair J, et al. (2004) Dynamic changes  
675 in c-raf phosphorylation and 14-3-3 protein binding in response to growth factor stim-  
676 ulation: differential roles of 14-3-3 protein binding sites. J Biol Chem 279: 14074–  
677 14086.
- 678 42. Dhillon AS, Yip YY, Grindlay GJ, Pakay JL, Dangers M, et al. (2009) The c-terminus  
679 of raf-1 acts as a 14-3-3-dependent activation switch. Cell Signal 21: 1645–1651.
- 680 43. Song JS, Gomez J, Stancato LF, Rivera J (1996) Association of a p95 vav-containing  
681 signaling complex with the fcepsiloniori gamma chain in the rbl-2h3 mast cell line.  
682 evidence for a constitutive in vivo association of vav with grb2, raf-1, and erk2 in an  
683 active complex. J Biol Chem 271: 26962–26970.
- 684 44. Costello PS, Walters AE, Mee PJ, Turner M, Reynolds LF, et al. (1999) The rho-  
685 family gtp exchange factor vav is a critical transducer of t cell receptor signals to the  
686 calcium, erk, and nf-kappab pathways. Proc Natl Acad Sci U S A 96: 3035–3040.
- 687 45. Graham D, Robertson C, Bautista J, Mascarenhas F, Diacovo M, et al. (2007)  
688 Neutrophil-mediated oxidative burst and host defense are controlled by a Vav-  
689 PLCgamma2 signaling axis in mice. J Clin Invest 117: 3445–3452.
- 690 46. Kim HS, Lim IK (2009) Phosphorylated extracellular signal-regulated protein kinases  
691 1 and 2 phosphorylate sp1 on serine 59 and regulate cellular senescence via tran-  
692 scription of p21sdi1/cip1/waf1. J Biol Chem 284: 15475–15486.
- 693 47. Milanini-Mongiat J, Pouyss?gur J, Pag?as G (2002) Identification of two sp1 phos-  
694 phorylation sites for p42/p44 mitogen-activated protein kinases: their implication in  
695 vascular endothelial growth factor gene transcription. J Biol Chem 277: 20631–  
696 20639.

- 697 48. Zhang Y, Cho YY, Petersen BL, Zhu F, Dong Z (2004) Evidence of stat1 phosphory-  
698 lation modulated by mapks, mek1 and msk1. *Carcinogenesis* 25: 1165–1175.
- 699 49. Li Z, Theus MH, Wei L (2006) Role of erk 1/2 signaling in neuronal differentiation of  
700 cultured embryonic stem cells. *Dev Growth Differ* 48: 513–523.
- 701 50. Yen A, Reece SL, Albright KL (1984) Dependence of hl-60 myeloid cell differentiation  
702 on continuous and split retinoic acid exposures: precommitment memory associated  
703 with altered nuclear structure. *J Cell Physiol* 118: 277–286.
- 704 51. Moon TS, Lou C, Tamsir A, Stanton BC, Voigt CA (2012) Genetic programs con-  
705 structed from layered logic gates in single cells. *Nature* 491: 249-53.
- 706 52. Wayman JA, Sagar A, Varner JD (2015) Dynamic modeling of cell-free biochemical  
707 networks using effective kinetic models. *Processes* 3: 138.
- 708 53. Igel C, Hansen N, Roth S (2007) Covariance matrix adaptation for multi-objective  
709 optimization. *Evol Comput* 15: 1-28.
- 710 54. Bezanson J, Edelman A, Karpinski S, Shah VB (2014) Julia: A fresh approach to  
711 numerical computing. *CoRR* abs/1411.1607.
- 712 55. Brooks SC, Kazmer S, Levin AA, Yen A (1996) Myeloid differentiation and retinoblas-  
713 toma phosphorylation changes in HL-60 cells induced by retinoic acid receptor- and  
714 retinoid X receptor-selective retinoic acid analogs. *Blood* 87: 227–237.
- 715 56. Rishi AK, Gerald TM, Shao ZM, Li XS, Baumann RG, et al. (1996) Regulation of the  
716 human retinoic acid receptor alpha gene in the estrogen receptor negative human  
717 breast carcinoma cell lines skbr-3 and mda-mb-435. *Cancer Res* 56: 5246-52.
- 718 57. Mueller BU, Pabst T, Fos J, Petkovic V, Fey MF, et al. (2006) Atra resolves the dif-  
719 ferentiation block in t(15;17) acute myeloid leukemia by restoring pu.1 expression.  
720 *Blood* 107: 3330-8.
- 721 58. Luo XM, Ross AC (2006) Retinoic acid exerts dual regulatory actions on the ex-  
722 pression and nuclear localization of interferon regulatory factor-1. *Exp Biol Med*

- 723 (Maywood) 231: 619-31.
- 724 59. Sylvester I, Schöler HR (1994) Regulation of the oct-4 gene by nuclear receptors.  
725 Nucleic Acids Res 22: 901-11.
- 726 60. Drach J, McQueen T, Engel H, Andreeff M, Robertson KA, et al. (1994) Retinoic  
727 acid-induced expression of cd38 antigen in myeloid cells is mediated through  
728 retinoic acid receptor-alpha. Cancer Res 54: 1746-52.
- 729 61. Liu M, Iavarone A, Freedman LP (1996) Transcriptional activation of the human  
730 p21(waf1/cip1) gene by retinoic acid receptor. correlation with retinoid induction of  
731 u937 cell differentiation. J Biol Chem 271: 31723-8.
- 732 62. Bunaciu RP, Yen A (2013) 6-formylindolo (3,2-b)carbazole (ficz) enhances retinoic  
733 acid (ra)-induced differentiation of hl-60 myeloblastic leukemia cells. Mol Cancer 12:  
734 39.
- 735 63. Balmer JE, Blomhoff R (2002) Gene expression regulation by retinoic acid. J Lipid  
736 Res 43: 1773-808.
- 737 64. Rosen ED, Hsu CH, Wang X, Sakai S, Freeman MW, et al. (2002) C/ebpalpha in-  
738 duces adipogenesis through ppargamma: a unified pathway. Genes Dev 16: 22-6.
- 739 65. Varley CL, Bacon EJ, Holder JC, Southgate J (2009) Foxa1 and irf-1 intermediary  
740 transcriptional regulators of ppargamma-induced urothelial cytodifferentiation. Cell  
741 Death Differ 16: 103-14.
- 742 66. Bruemmer D, Yin F, Liu J, Berger JP, Sakai T, et al. (2003) Regulation of the growth  
743 arrest and dna damage-inducible gene 45 (gadd45) by peroxisome proliferator-  
744 activated receptor gamma in vascular smooth muscle cells. Circ Res 93: e38-47.
- 745 67. Delerive P, De Bosscher K, Besnard S, Vanden Berghe W, Peters JM, et al. (1999)  
746 Peroxisome proliferator-activated receptor alpha negatively regulates the vascular  
747 inflammatory gene response by negative cross-talk with transcription factors nf-  
748 kappaB and ap-1. J Biol Chem 274: 32048-54.

- 749 68. Altioik S, Xu M, Spiegelman BM (1997) Ppargamma induces cell cycle withdrawal:  
750 inhibition of e2f/dp dna-binding activity via down-regulation of pp2a. Genes Dev 11:  
751 1987-98.
- 752 69. Fei J, Cook C, Gillespie M, Yu B, Fullen K, et al. (2011) Atherogenic  $\omega$ -6 lipids mod-  
753 ulate ppar- egr-1 crosstalk in vascular cells. PPAR Res 2011: 753917.
- 754 70. Song EK, Lee YR, Kim YR, Yeom JH, Yoo CH, et al. (2012) Naadp mediates insulin-  
755 stimulated glucose uptake and insulin sensitization by ppar $\gamma$  in adipocytes. Cell Rep  
756 2: 1607-19.
- 757 71. Szanto A, Nagy L (2005) Retinoids potentiate peroxisome proliferator-activated re-  
758 ceptor gamma action in differentiation, gene expression, and lipid metabolic pro-  
759 cesses in developing myeloid cells. Mol Pharmacol 67: 1935-43.
- 760 72. Han S, Sidell N, Fisher PB, Roman J (2004) Up-regulation of p21 gene expres-  
761 sion by peroxisome proliferator-activated receptor gamma in human lung carcinoma  
762 cells. Clin Cancer Res 10: 1911-9.
- 763 73. Von Knethen A, Brüne B (2002) Activation of peroxisome proliferator-activated re-  
764 ceptor gamma by nitric oxide in monocytes/macrophages down-regulates p47phox  
765 and attenuates the respiratory burst. J Immunol 169: 2619-26.
- 766 74. Dispirito JR, Fang B, Wang F, Lazar MA (2013) Pruning of the adipocyte peroxisome  
767 proliferator-activated receptor  $\gamma$  cistrome by hematopoietic master regulator pu.1.  
768 Mol Cell Biol 33: 3354-64.
- 769 75. Chen H, Ray-Gallet D, Zhang P, Hetherington CJ, Gonzalez DA, et al. (1995) Pu.1  
770 (spi-1) autoregulates its expression in myeloid cells. Oncogene 11: 1549-60.
- 771 76. Steidl U, Rosenbauer F, Verhaak RGW, Gu X, Ebralidze A, et al. (2006) Essential  
772 role of jun family transcription factors in pu.1 knockdown-induced leukemic stem  
773 cells. Nat Genet 38: 1269-77.
- 774 77. Pahl HL, Scheibe RJ, Zhang DE, Chen HM, Galson DL, et al. (1993) The proto-

- 775 oncogene pu.1 regulates expression of the myeloid-specific cd11b promoter. J Biol  
776 Chem 268: 5014-20.
- 777 78. Yuki H, Ueno S, Tatetsu H, Niiro H, Iino T, et al. (2013) Pu.1 is a potent tumor  
778 suppressor in classical hodgkin lymphoma cells. Blood 121: 962-70.
- 779 79. Li SL, Schlegel W, Valente AJ, Clark RA (1999) Critical flanking sequences of pu.1  
780 binding sites in myeloid-specific promoters. J Biol Chem 274: 32453-60.
- 781 80. Timchenko N, Wilson DR, Taylor LR, Abdelsayed S, Wilde M, et al. (1995) Autoreg-  
782 ulation of the human c/ebp alpha gene by stimulation of upstream stimulatory factor  
783 binding. Mol Cell Biol 15: 1192-202.
- 784 81. Lidonnici MR, Audia A, Soliera AR, Prisco M, Ferrari-Amorotti G, et al. (2010) Ex-  
785 pression of the transcriptional repressor gfi-1 is regulated by c/ebpalpha and is  
786 involved in its proliferation and colony formation-inhibitory effects in p210bcr/abl-  
787 expressing cells. Cancer Res 70: 7949-59.
- 788 82. D'Alo' F, Johansen LM, Nelson EA, Radomska HS, Evans EK, et al. (2003) The  
789 amino terminal and e2f interaction domains are critical for c/ebp alpha-mediated  
790 induction of granulopoietic development of hematopoietic cells. Blood 102: 3163-  
791 71.
- 792 83. Pan Z, Hetherington CJ, Zhang DE (1999) Ccaat/enhancer-binding protein activates  
793 the cd14 promoter and mediates transforming growth factor beta signaling in mono-  
794 cyte development. J Biol Chem 274: 23242-8.
- 795 84. Harris TE, Albrecht JH, Nakanishi M, Darlington GJ (2001) Ccaat/enhancer-binding  
796 protein-alpha cooperates with p21 to inhibit cyclin-dependent kinase-2 activity and  
797 induces growth arrest independent of dna binding. J Biol Chem 276: 29200-9.
- 798 85. Bauvois B, Durant L, Laboureau J, Barthélémy E, Rouillard D, et al. (1999) Upreg-  
799 ulation of cd38 gene expression in leukemic b cells by interferon types i and ii. J  
800 Interferon Cytokine Res 19: 1059-66.

- 801 86. Passioura T, Dolnikov A, Shen S, Symonds G (2005) N-ras-induced growth suppres-  
802 sion of myeloid cells is mediated by irf-1. *Cancer Res* 65: 797-804.
- 803 87. Dahl R, Iyer SR, Owens KS, Cuylear DD, Simon MC (2007) The transcriptional  
804 repressor gfi-1 antagonizes pu.1 activity through protein-protein interaction. *J Biol  
805 Chem* 282: 6473-83.
- 806 88. Duan Z, Horwitz M (2003) Targets of the transcriptional repressor oncoprotein gfi-1.  
807 *Proc Natl Acad Sci U S A* 100: 5932-7.
- 808 89. Chen H, Zhang P, Radomska HS, Hetherington CJ, Zhang DE, et al. (1996) Octamer  
809 binding factors and their coactivator can activate the murine pu.1 (spi-1) promoter.  
810 *J Biol Chem* 271: 15743-52.
- 811 90. Behre G, Whitmarsh AJ, Coghlan MP, Hoang T, Carpenter CL, et al. (1999) c-jun  
812 is a jnk-independent coactivator of the pu.1 transcription factor. *J Biol Chem* 274:  
813 4939-46.
- 814 91. Kardassis D, Papakosta P, Pardali K, Moustakas A (1999) c-jun transactivates the  
815 promoter of the human p21(waf1/cip1) gene by acting as a superactivator of the  
816 ubiquitous transcription factor sp1. *J Biol Chem* 274: 29572-81.
- 817 92. Johnson DG, Ohtani K, Nevins JR (1994) Autoregulatory control of e2f1 expression  
818 in response to positive and negative regulators of cell cycle progression. *Genes Dev*  
819 8: 1514-25.
- 820 93. Fu M, Zhang J, Lin Y, Zhu X, Ehrengruber MU, et al. (2002) Early growth response  
821 factor-1 is a critical transcriptional mediator of peroxisome proliferator-activated  
822 receptor-gamma 1 gene expression in human aortic smooth muscle cells. *J Biol  
823 Chem* 277: 26808-14.
- 824 94. Mak KS, Funnell APW, Pearson RCM, Crossley M (2011) Pu.1 and haematopoietic  
825 cell fate: Dosage matters. *Int J Cell Biol* 2011: 808524.
- 826 95. Chen F, Wang Q, Wang X, Studzinski GP (2004) Up-regulation of egr1 by 1,25-

- 827 dihydroxyvitamin d3 contributes to increased expression of p35 activator of cyclin-  
828 dependent kinase 5 and consequent onset of the terminal phase of hl60 cell differ-  
829 entiation. *Cancer Res* 64: 5425-33.
- 830 96. Suh J, Jeon YJ, Kim HM, Kang JS, Kaminski NE, et al. (2002) Aryl hydrocarbon  
831 receptor-dependent inhibition of ap-1 activity by 2,3,7,8-tetrachlorodibenzo-p-dioxin  
832 in activated b cells. *Toxicol Appl Pharmacol* 181: 116-23.
- 833 97. Shen M, Bunaciu RP, Congleton J, Jensen HA, Sayam LG, et al. (2011) Inter-  
834 feron regulatory factor-1 binds c-cbl, enhances mitogen activated protein kinase  
835 signaling and promotes retinoic acid-induced differentiation of hl-60 human myelo-  
836 monoblastic leukemia cells. *Leuk Lymphoma* 52: 2372-9.
- 837 98. Bunaciu RP, Yen A (2011) Activation of the aryl hydrocarbon receptor ahr promotes  
838 retinoic acid-induced differentiation of myeloblastic leukemia cells by restricting ex-  
839 pression of the stem cell transcription factor oct4. *Cancer Res* 71: 2371-80.
- 840 99. Jackson DA, Pombo A, Iborra F (2000) The balance sheet for transcription: an anal-  
841 ysis of nuclear rna metabolism in mammalian cells. *FASEB J* 14: 242-54.
- 842 100. Zhao ZW, Roy R, Gebhardt JCM, Suter DM, Chapman AR, et al. (2014) Spatial orga-  
843 nization of rna polymerase ii inside a mammalian cell nucleus revealed by reflected  
844 light-sheet superresolution microscopy. *Proc Natl Acad Sci U S A* 111: 681-6.
- 845 101. Freitas R, Merkle R (2004) Kinematic Self-Replicating Machines. Oxford University  
846 Press.
- 847 102. Yang E, van Nimwegen E, Zavolan M, Rajewsky N, Schroeder M, et al. (2003) De-  
848 cay rates of human mrnas: correlation with functional characteristics and sequence  
849 attributes. *Genome Res* 13: 1863-72.
- 850 103. Doherty MK, Hammond DE, Clague MJ, Gaskell SJ, Beynon RJ (2009) Turnover  
851 of the human proteome: determination of protein intracellular stability by dynamic  
852 silac. *J Proteome Res* 8: 104-12.

- 853 104. Darzacq X, Shav-Tal Y, de Turris V, Brody Y, Shenoy SM, et al. (2007) In vivo dy-  
854 namics of rna polymerase ii transcription. Nat Struct Mol Biol 14: 796-806.
- 855 105. Boström K, Wettsten M, Borén J, Bondjers G, Wiklund O, et al. (1986) Pulse-chase  
856 studies of the synthesis and intracellular transport of apolipoprotein b-100 in hep g2  
857 cells. J Biol Chem 261: 13800-6.
- 858 106. Meyers R, editor (2004) Encyclopedia of Molecular Cell Biology and Molecular  
859 Medicine, Volume 1, 2nd Edition. ISBN: 978-3-527-30543-8. Wiley-Blackwell.
- 860 107. Rosenbluth MJ, Lam WA, Fletcher DA (2006) Force microscopy of nonadherent  
861 cells: a comparison of leukemia cell deformability. Biophys J 90: 2994-3003.

**Table 1:** Myelomonocytic transcription factor connectivity used in the signal integration and phenotype modules.

862

863

Effector	Effect	Target	Source
RAR $\alpha$	+	RAR $\alpha$	(56)
	+	PU.1	(57)
	+	C/EBP $\alpha$	(36)
	+	IRF-1	(58)
	-	Oct4	(59)
	+	CD38	(60)
	+	p21	(61)
	+	AhR	(62)
	+	EGR1	(63)
PPAR $\gamma$	+	C/EBP $\alpha$	(64)
	+	IRF-1	(65)
	+	Oct1	(66)
	-	AP-1	(67)
	-	E2F	(68)
	-	EGR1	(69)
	+	CD38	(70)
	+	CD14	(71)
	+	p21	(72)
	-	p47phox	(73)
PU.1	-	PPAR $\gamma$	(74)
	+	PU.1	(75)
	+	AP-1	(76)
	+	EGR1	(32)
	+	CD11b	(77)
	+	p21	(78)
	+	p47phox	(79)
C/EBP $\alpha$	+	PPAR $\gamma$	(64)
	+	PU.1	(37)
	+	C/EBP $\alpha$	(80)
	+	Gfi-1	(81)
	-	E2F	(82)
	+	CD14	(83)

	+	p21	(84)
IRF-1	+	CD38	(85)
	+	p21	(86)
	-	PU.1	(87)
	-	C/EBP $\alpha$	(88)
	-	E2F	(88)
	-	EGR1	(32)
	-	p21	(88)
Oct1	+	PU.1	(89)
AP-1	-	PPAR $\gamma$	(67)
	+	PU.1	(90)
	+	p21	(91)
E2F	+	E2F	(92)
EGR1	+	PPAR $\gamma$	(93)
	-	Gfi-1	(94)
	+	CD14	(95)
AhR	+	AP-1	(96)
	+	IRF-1	(97)
	-	Oct4	(98)
	-	PU.1	

**Table 2:** Characteristic model parameters estimated from literature.

Symbol	Description	Value	Units	Source
$R_1$	RNA polymerase abundance	75,000	copies/cell	(99, 100)
$R_2$	Ribosome abundance	$1 \times 10^6$	copies/cell	(101)
$G_i$	Characteristic gene abundance	2	copies/cell	this study
$K_X$	Saturation constant transcription	4,600	copies/cell	this study
$K_T$	Saturation constant translation	100,000	copies/cell	this study
$t_{1/2,m}$	characteristic mRNA half-life (transcription factor)	2	hr	(102)
$t_{1/2,p}$	characteristic protein half-life	10	hr	(103)
$\theta_{m,j}$	characteristic mRNA degradation constant	0.34	$hr^{-1}$	derived
$\theta_{p,j}$	characteristic protein degradation constant	0.07	$hr^{-1}$	derived
866				
$t_d$	HL-60 doubling time	19.5	hr	this study
$\mu$	growth rate	0.035	$hr^{-1}$	derived
$k_d$	death rate	$0.10\mu$	$hr^{-1}$	derived
$e_T$	elongation rate RNA polymerase	6	nt/s	(104)
$e_X$	elongation rate Ribosome	5	aa/s	(105)
$L_{T,o}$	characteristic gene length	15,000	nt	(106)
$L_{X,o}$	characteristic transcript length	5,000	nt	derived
$k_T$	characteristic transcription rate	1.44	$hr^{-1}$	derived
$k_X$	characteristic translation rate	3.60	$hr^{-1}$	derived
$D$	Diameter of an HL-60 cell	12.4	$\mu m^3$	(107)
$f_C$	cytoplasmic fraction	0.51	dimensionless	(107)

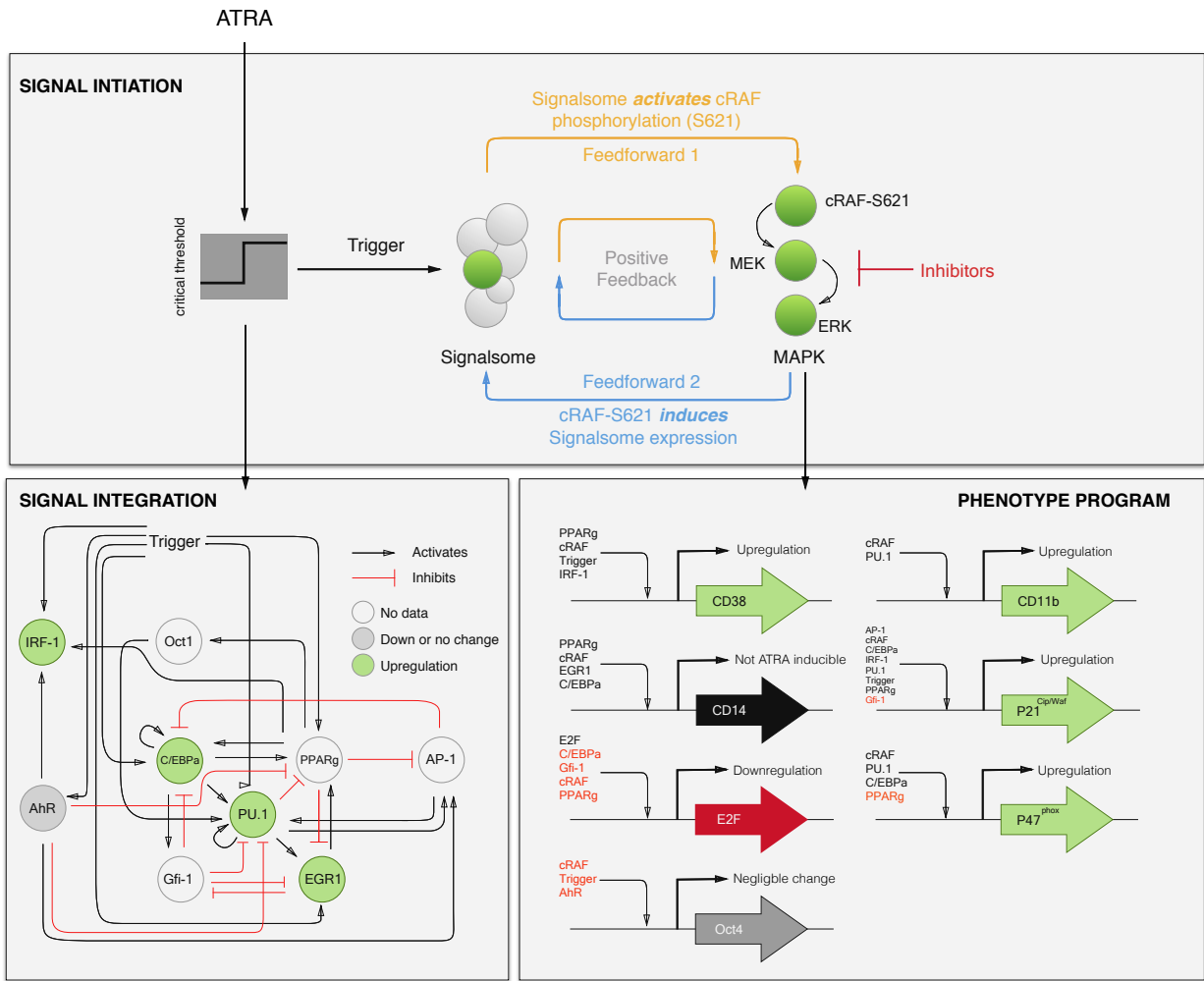


**Fig. 1:** Schematic of the effective ATRA differentiation circuit. Above a critical threshold, ATRA activates an upstream Trigger, which induces signalsome complex formation. Signalsome activates the mitogen-activated protein kinase (MAPK) cascade which in turn drives the differentiation program and signalsome formation. Both Trigger and activated cRaf-pS621 drive a phenotype gene expression program responsible for differentiation. Trigger activates the expression of a series of transcription factors which in combination with cRaf-pS621 result in phenotypic change.

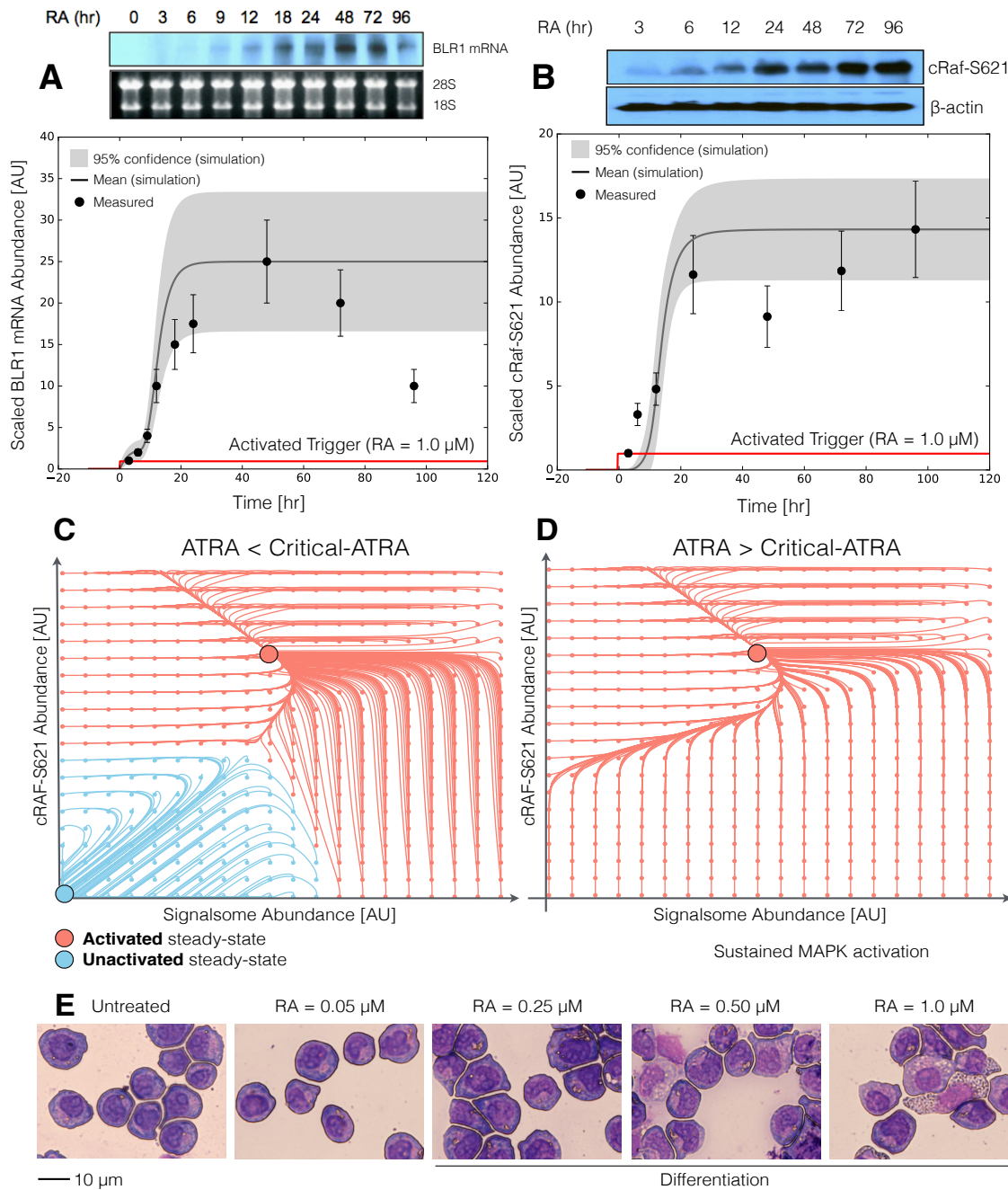


**Fig. 2:** Model analysis for ATRA-induced HL-60 differentiation. A: BLR1 mRNA versus time following exposure to  $1\mu\text{M}$  ATRA at  $t = 0$  hr. B: cRaf-pS621 versus time following exposure to  $1\mu\text{M}$  ATRA at  $t = 0$  hr. Points denote experimental measurements, solid lines denote the mean model performance. Shaded regions denote the 99% confidence interval calculated over the parameter ensemble. C: Signalsome and cRaf-pS621 nullclines for ATRA below the critical threshold. The model had two stable steady states and a single unstable state in this regime. D: Signalsome and cRaf-pS621 nullclines for ATRA above the critical threshold. In this regime the model had only a single stable steady state. E: Morphology of HL-60 as a function of ATRA concentration ( $t = 72$  hr).

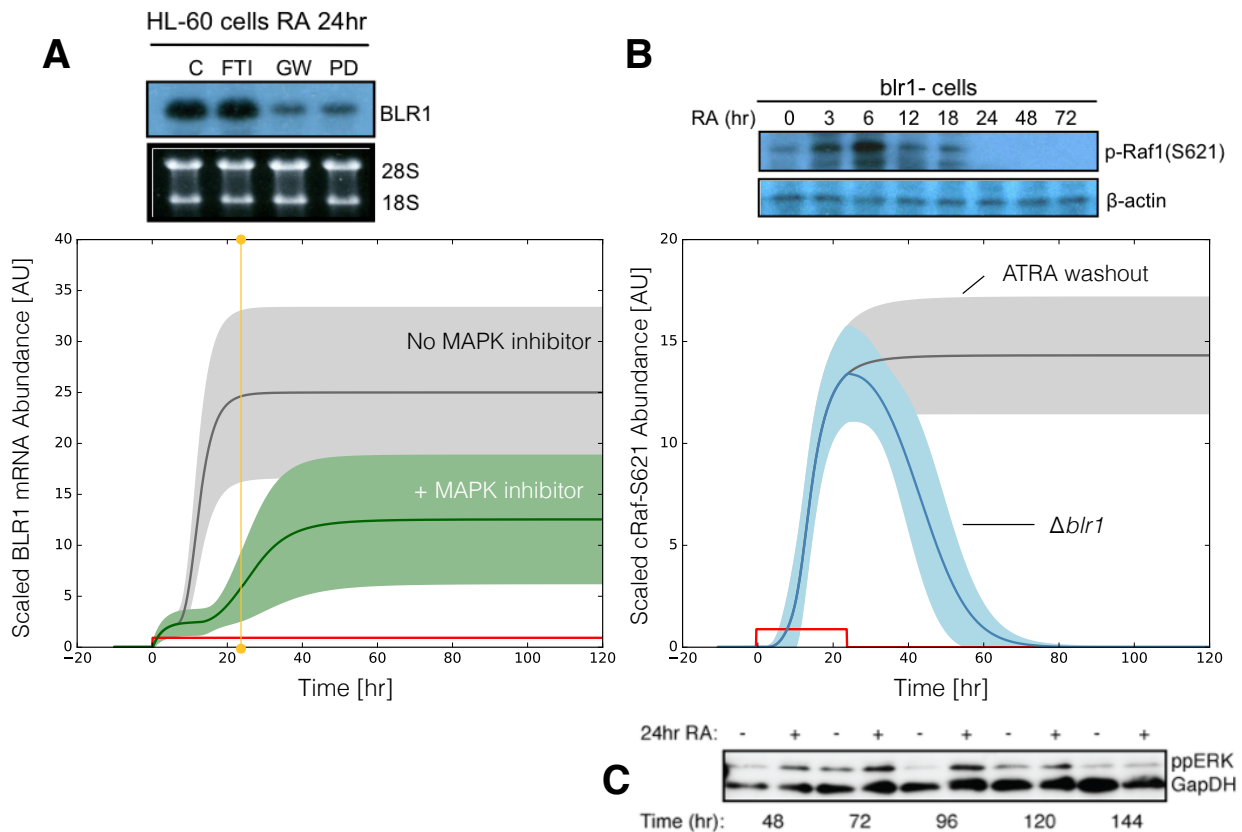


**Fig. 3:** Model simulation following exposure to  $1\mu\text{M}$  ATRA. A: BLR1 mRNA versus time with and without MAPK inhibitor. B: cRaf-pS621 versus time following pulsed exposure to  $1\mu\text{M}$  ATRA with and without BLR1. Solid lines denote the mean model performance, while shaded regions denote the 99% confidence interval calculated over the parameter ensemble. C: Western blot analysis of phosphorylated ERK1/2 in ATRA washout experiments. Experimental data in panels A and B were reproduced from Wang and Yen (20), data in panel C is reported in this study.

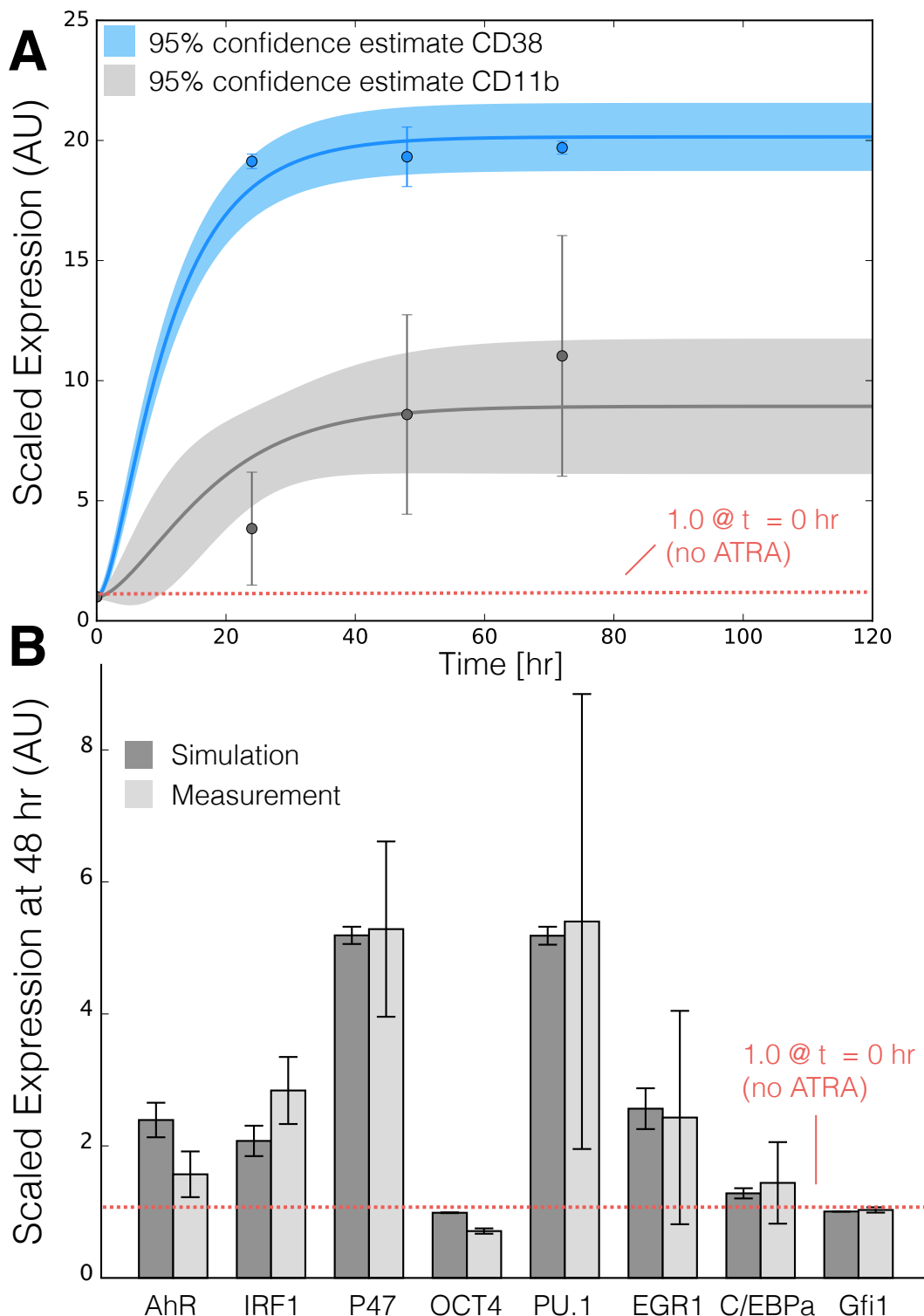


**Fig. 4:** Model simulation of the HL-60 gene expression program following exposure to  $1\mu\text{M}$  ATRA at  $t = 0$  hr. A: CD38 and CD11b expression versus time following ATRA exposure at time  $t = 0$  hr. B: Gene expression at  $t = 48$  hr following ATRA exposure. Experimental data in panels A and B were reproduced from Jensen et al. (25).

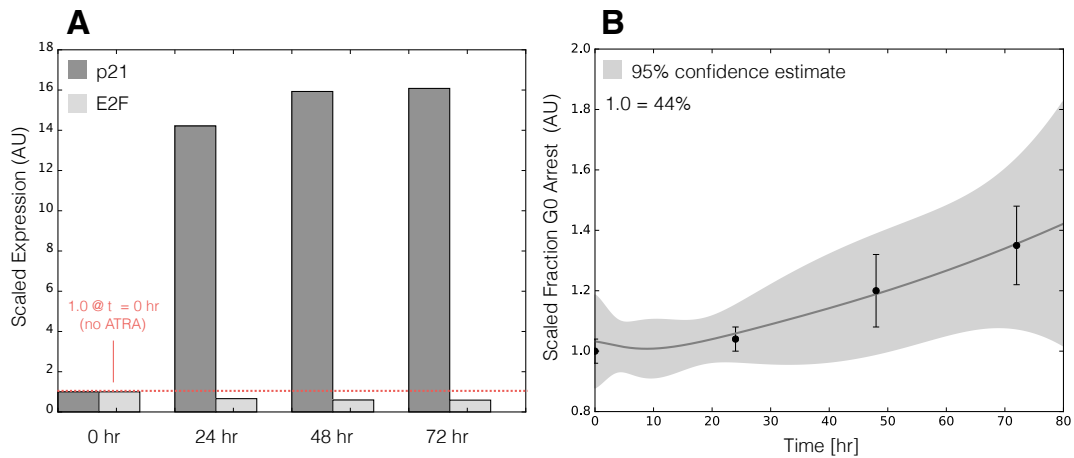


**Fig. 5:** Model simulation of HL-60 cell-cycle arrest following exposure to  $1\mu\text{M}$  ATRA at  $t = 0$  hr. A: Predicted p21 and E2F expression levels for the best parameter set following ATRA exposure at time  $t = 0$  hr. B: Estimated fraction of HL-60 cells in G0 arrest following ATRA exposure at time  $t = 0$  hr. The gray region denotes the 95% confidence estimate of the polynomial model. Experimental data in panel B was reproduced from Jensen et al. (25).

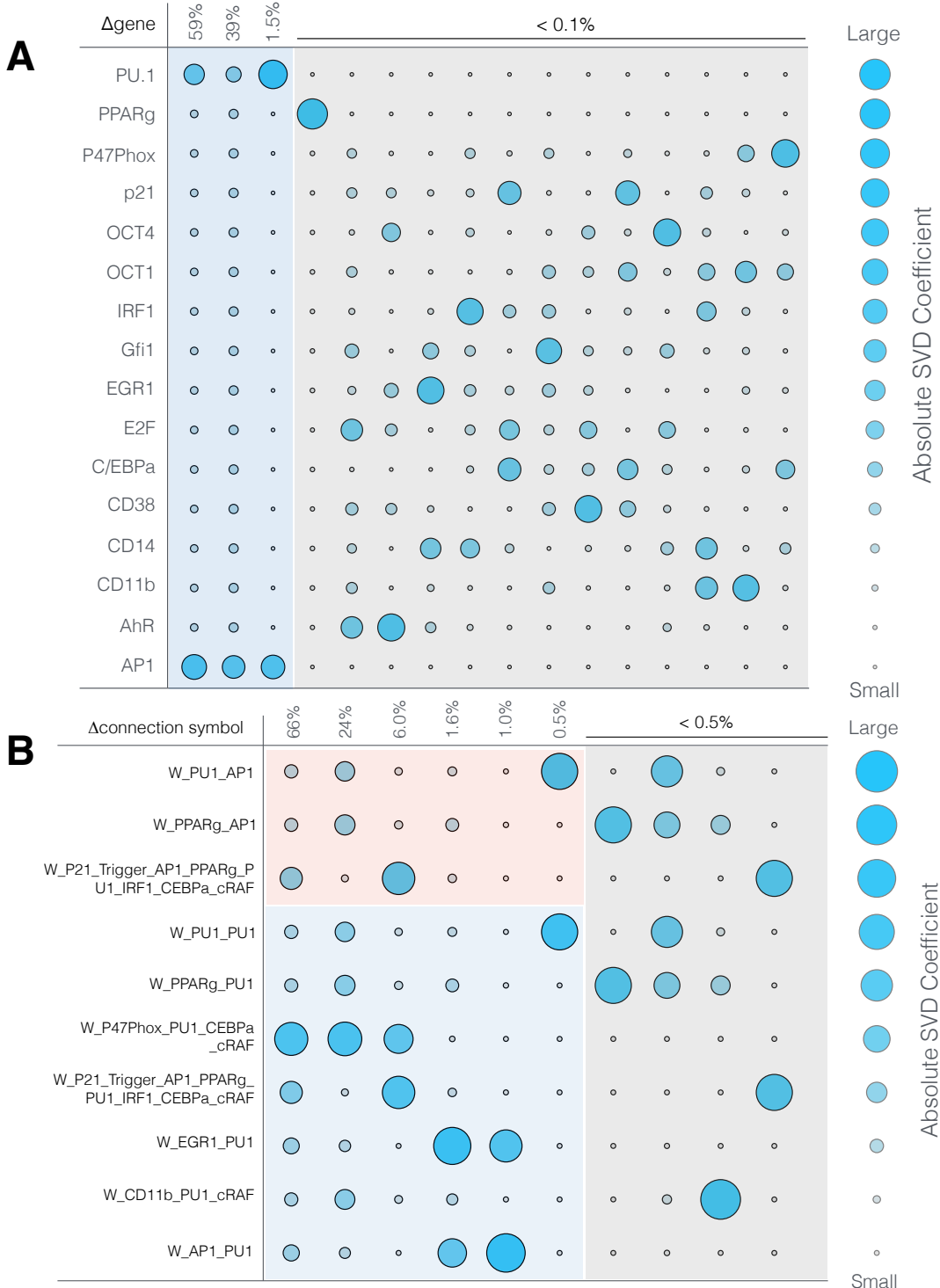


**Fig. 6:** Robustness of the HL-60 differentiation program following exposure to  $1\mu\text{M}$  ATRA at  $t = 0$  hr. A: Singular value decomposition of the system response ( $l^2$ -norm between the perturbed and nominal state) following pairwise gene knockout simulations using the best fit parameter set. The percentage at the top of each column describes the fraction of the variance in the system state captured by the node combinations in the rows. B: Singular value decomposition of the system response ( $l^2$ -norm between the perturbed and nominal state) following the pairwise removal of connections from the PU.1 and AP1 nodes.

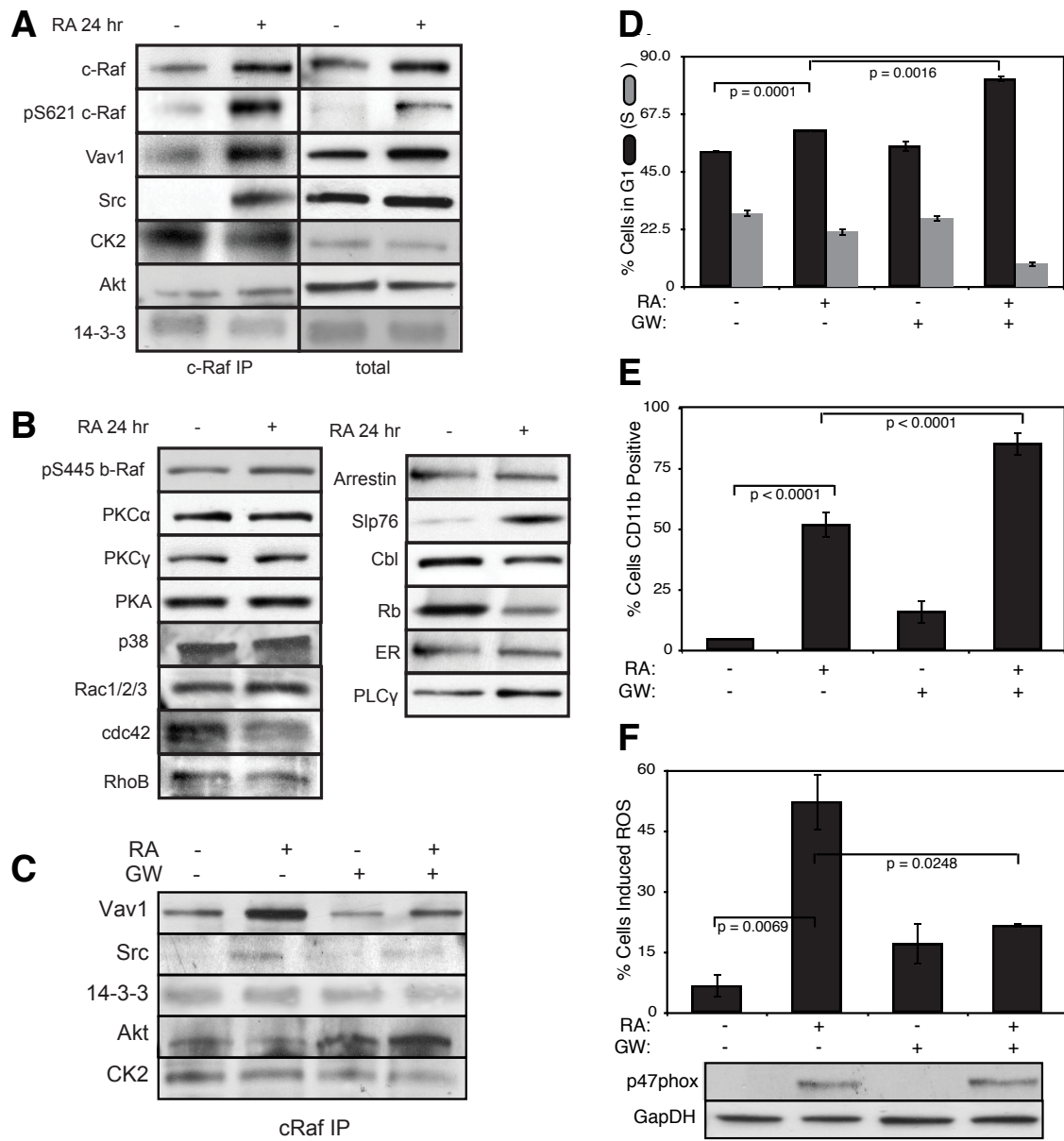


**Fig. 7:** Investigation of a panel of possible Raf interaction partners in the presence and absence of ATRA. A: Species identified to precipitate out with Raf: first column shows Western blot analysis on total Raf immunoprecipitation with and without 24 hr ATRA treatment and the second on total lysate. B: The expression of species considered that did not precipitate out with Raf at levels detectable by Western blot analysis on total lysate. C: Effect of the Raf inhibitor GW5074 on Raf interactions as determined by Western blot analysis of total Raf immunoprecipitation. The Authors note the signal associated with Src was found to be weak. D: Cell Cycle distribution as determined by flow cytometry indicated arrest induced by ATRA, which was increased by the addition of GW5074. E: Expression of the cell surface marker CD11b as determined by flow cytometry indicated increased expression induced by ATRA, which was enhanced by the addition of GW5074. F: Inducible reactive oxygen species (ROS) as determined by DCF flow cytometry. The functional differentiation response of ATRA treated cells was mitigated by GW5074.